Thermal–electrical model for energy estimation of a water cooled photovoltaic module

Filippo Spertino [a,*], Antonio D'Angola [b], Diana Enescu [c], Paolo Di Leo [a], Giovanni Vincenzo Fracastoro [a], Renato Zaffina [b]

[a] *Politecnico di Torino, Energy Department, Corso Duca degli Abruzzi 24, 10129 Torino, Italy*
[b] *Università degli Studi della Basilicata, Scuola di Ingegneria, Via dell'Ateneo Lucano 10, 85100 Potenza, Italy*
[c] *Valahia University of Targoviste, Department of Electronics, Telecommunications and Energy, Targoviste, Dambovita, Romania*

Abstract

In this paper a theoretical model, which integrates both thermal and electrical aspects, has been developed in order to analyze an unglazed Photovoltaic (PV) module with water cooling. The coolant flow induces higher conversion efficiency due to lower temperatures. However, a non-uniform temperature field of solar cells arises with a consequent impact on their electrical parameters and the corresponding power losses are investigated. Outdoor experimental tests have been carried out to indirectly estimate the temperature of the solar cells at known conditions of irradiance and ambient temperature and to characterize the PV module at Standard Test Conditions (STC). In the outdoor characterization of commercial PV modules without cooling, the current–voltage curves are corrected to STC with a standard procedure, for comparing them with the manufacturer datasheets. In this paper, it is experimentally verified that the STC can be reasonably reproduced in the field in clear sky conditions thanks to a suitable cooling. Finally, by means of daily simulations, the performance improvement with variable coolant flow rates, for two reference sites at different climates, is investigated in details.

Keywords: Photovoltaic modules; Thermal–electrical model; Water cooling; Experimental tests

1. Introduction

Only a fraction of solar radiation is converted by Photovoltaic (PV) systems into electricity, while a large part of the thermal energy is wasted and contributes to the increase of solar (or PV) cell temperature. As a consequence, the electrical efficiency drops (Platz et al., 1997; Kalogirou and Tripanagnostopoulos, 2006; Chow, 2010; Spertino et al., 2014) because the performance of solar cells depends on their ambient conditions, among which the cell operating temperature plays a major role. In general, the PV efficiency loss with temperature depends on the type of cell. A linear dependence of the electrical performance on the operating temperature has been indicated in various references (Kawamura et al., 1997; Omubo-Pepple et al., 2009; Suresh et al., 2013). An indicative value reported in SEI (2004) for the reduction of crystalline silicon (c-Si) efficiency with unitary temperature increment of the solar cell

* Corresponding author. Tel.: +39 011 090 7120; fax: +39 011 090 7199.
E-mail addresses: filippo.spertino@polito.it (F. Spertino), antonio.dangola@unibas.it (A. D'Angola), diana.enescu@valahia.ro (D. Enescu), paolo.dileo@polito.it (P. Di Leo), giovanni.fracastoro@polito.it (G.V. Fracastoro), renzaff@gmail.com (R. Zaffina).

Nomenclature

Acronyms

AM	Air Mass
ARC	Anti Reflective Coating
CHP	Combined Heat and Power
DC	direct current
MPP	Maximum Power Point
NOCT	Nominal Operating Cell Temperature
PC	polycarbonate
PCM	phase change material
PV	Photovoltaic
PV/T	Photovoltaic–Thermal
SAHP	Solar Assisted Heat Pump
STC	Standard Test Conditions
TE	thermoelectric
TPU	thermoplastic polyurethane

Symbols

$\mathbf{A}$	matrix
A	heat transfer surface (m^2)
$\mathbf{b}$	vector
c	specific heat of water ($J\,kg^{-1}\,K^{-1}$)
d	hydraulic diameter of water flows passage (m)
E_G	energy gap (eV)
E_{G0}	energy gap at 0 K (eV)
G	solar irradiance ($W\,m^{-2}$)
h	surface heat transfer coefficient ($W\,m^{-2}\,K^{-1}$)
I	current (A)
k	thermal conductivity ($W\,m^{-1}\,K^{-1}$)
K_{ph}	spectral-response parameter
m	diode ideality factor
n	step counter
p	perimeter (m)
P	electric power (W)
q	electron charge ($1.60217646 \cdot 10^{-19}$ C)
$\dot{q}$	heat flux ($W\,m^{-2}$)
R	module electrical resistance (Ω)
s	thickness (m)
S	surface (m^2)
SR	spectral response ($A\,W^{-1}$)
T	temperature (K)
T_{sky}	sky temperature (K)
U	overall heat transfer coefficient ($W\,m^{-2}\,K^{-1}$)
$\dot{v}$	volume flow rate of water ($l\,h^{-1}$)
V	voltage (V)
x, y, z	space variables
$\mathbf{x}$	vector for linear system solution
X, Y	height and width of the alveolar polycarbonate layer (m)
w	water velocity ($m\,s^{-1}$)
Z	space derivative of the water temperature ($K\,m^{-1}$)

Greek symbols

α	absorptivity (–)
α_{Isc}	short-circuit current coefficient ($A\,°C^{-1}$)
β	tilt angle of PV module (°)
β_{Uoc}	open-circuit voltage coefficient ($V\,°C^{-1}$)
γ_P	maximum power coefficient ($\%\,°C^{-1}$)
δ	power increase (%)
ε	polycarbonate emissivity (–)
η	efficiency (–)
κ	Boltzmann constant ($1.3806503 \cdot 10^{-23}\,J\,K^{-1}$)
λ	wavelength (μm)
μ	dynamic viscosity of water ($kg\,s^{-1}\,m^{-1}$)
ν	kinematic viscosity of water ($m^2\,s^{-1}$)
ξ	real power gain (%)
ρ	density ($kg\,m^{-3}$)
σ	Stefan–Boltzmann constant ($5.67 \cdot 10^{-8}\,W\,m^{-2}\,K^{-4}$)
τ	transmissivity (–)
φ	constant depending on the cell material
Φ	solar spectral emissive power ($W\,m^{-2}\,\mu m^{-1}$)
χ	power loss (%)
ψ	constant depending on the cell material

Superscripts

T	transposition
iso	isothermal

Subscripts

a	ambient
alv	alveolar
ag	air–gap
C	cell
c	cross-sectional
cond	conductive
conv	convective
D	diode
el	electrical
G	gap
I	ideal
in	input
inw	inlet water
max	maximum
mpp	at maximum power
NC	without coolant
oc	open-circuit
pc	polycarbonate
ph	photo-generated
PVm	PV module
R	real
rad	radiative
ref	reference value, at reference temperature
s	surface
ser	series
sc	short-circuit
sh	shunt
t	thermal
w	water
0	reverse saturation

is $-0.5\ \%\ °C^{-1}$, similar to the value ($-0.45\%\ °C^{-1}$) found by Skoplaki and Palyvos (2009). In particular, there is a reduction of both operating voltages (both at open circuit and maximum power conditions) and fill factor, but a slight increase in the short-circuit current (Zondag, 2008).

For this reason, it is necessary to improve the heat dissipation of the PV module (Ye et al., 2013; Du et al., 2013).

In the previous years, many theoretical and experimental studies have been performed in order to design cooling systems for PV modules. One of the most efficient solutions is to combine a standard PV module with a liquid flow heat exchanger into a hybrid Photovoltaic/Thermal (PV/T) system. Following this approach, it is possible to produce at the same time warm water and electricity with better electrical conversion efficiency due to lower cell temperature. This is an interesting example of a simple, clean and potentially cheap Combined Heat and Power (CHP) system, which is particularly useful when a limited roof space is available.

A contribution by Zondag et al. (2003) reported the results of comparing a conventional PV module, an unglazed PV/T module and a glazed PV/T module, resulting in average annual electrical efficiency values of 7.2%, 7.6% and 6.6%, respectively.

In the unglazed solution included in the integrated solar home system presented in Krauter (2004), the PV module is connected to a water tank that provides the PV system cooling by using an "extended heat capacity". The cooling effect determines a temperature reduction of about 20 °C with respect to a conventional system, leading to an electrical yield increase of about 9–12%.

In this paper, a prototype mono-crystalline silicon module has been tested to investigate the profitability of water-cooling for higher efficiency and plastic-laminated sandwich for lower weight instead of glass. Water cooling provides the possibility to reproduce testing conditions close to Standard Test Conditions (STC) which normally are not found in practice. This paper addresses a number of aspects referring to the characterization of this PV module, referring to its structure, electrical and thermal models, and performance assessment.

The next sections of this paper are organized as follows: Section 2 recalls the distinction between passive and active methods for PV panel cooling. Section 3 describes the structure of the unconventional PV module and discusses the effects of water cooling on the module. Section 4 illustrates the theoretical thermal–electrical models. Section 5 contains the characterization of the module by reproducing the STC directly in outdoor experimental tests. Section 6 reports some numerical results regarding two reference sites with suitable range of coolant flow rates. Section 7 presents the conclusions.

2. Methods for PV module cooling

There are two methods used for cooling the PV modules, namely:

- *Passive cooling*, requiring natural means associated with specific design solutions to improve the heat removal from the PV module, without requiring the use of energy.
- *Active cooling*, using thermal control systems and devices requiring additional energy to power these control systems and devices.

The basic cooling media for both passive and active cooling systems are air and water. Due to its thermal properties, air is less efficient than water as cooling medium (Xu et al., 2009). In order to obtain a similar level of efficiency from an air cooling system with respect to the water cooling system, the energy consumption to supply the fan in the air cooling system has to be higher than the energy consumption of the pump used in the water cooling system. Active and passive cooling systems may coexist in order to obtain better efficiency (Makki et al., 2015).

The analysis carried out in this study refers to PV systems without solar concentration and without recovering the heat for thermal uses; the heat originating from cooling the PV module is wasted to the ambient.

The characteristics of active and passive cooling systems taken from recent literature contributions are summarized below.

For passive cooling, heat is carried away from the PV cells and is rejected into the environment (e.g., by natural convection) (Royne et al., 2005). Classical design structures require ducts, heat pipes or additional fins behind the PV cell to make the natural circulation of air or water easier (Brinkworth and Sandberg, 2006; Chen et al., 2014). A comprehensive review of the methods used for thermal management of PV systems has been provided in Makki et al. (2015), by considering different cooling means like air, heat pipes, liquids, thermoelectric (TE) devices, and phase change materials (PCMs).

Active cooling is in general used both for achieving higher electrical efficiency of PV cell and for making heat available to nearby users. It is based on heat extraction by using devices like fans to force air, or pumps to circulate water to the backside of the PV modules (Bahaidarah et al., 2013), for example by using circulating cooling water which flows across a thermally conductive tube on which the PV cells are placed (Lasich, 2002). Water spraying is also considered in some applications for PV module cooling (Abdolzadeh and Ameri, 2009; Salih et al., 2015), especially in arid regions with water scarcity (Moharram et al., 2013). Active cooling systems enhance the heat transfer, typically by convection. Active cooling is effective only when the overall energy production increase is higher than the energy consumption of the cooling device (Makki et al., 2015). Another example of active cooling is illustrated in Ueda et al. (2008), describing a water-cooled PV system, with floating PV modules placed on the surface of a lake, transferring power through DC cables to the inverters mounted on the ground. The PV modules are cooled by using a pump that draws water from the lake and a spray

system operating during the day. Comparison with a similar system placed on the ground leads to temperatures of the PV system mounted on the lake 20 °C lower (and daily energy output 12% higher) than for the PV modules located on the ground. The pump consumption is relatively low, making the cooling system quite effective.

Zhao et al. (2011) presents a PV/evaporator roof modules-based heat pump system which operates at 10 °C evaporation and 60 °C condensation temperature, to provide both electricity and space heating to buildings. The results showed that this system can bring significant improvement in thermal and electrical efficiencies. Under the Nottingham (UK) operating condition, the module obtained a thermal efficiency of 55% and an electrical efficiency of 19%, while the module based on heat pump system obtained an overall efficiency above 70%. Evaporative coolers are used in Leow et al. (2014) for decreasing the PV module temperature and raising the power output. A direct current (DC) hybrid cooling system is used, in which the air is maintained in constant motion by means of a DC brushless fan, and a water pump maintains the water circulation at the backside and front surface of the PV module. The fan and the water pump are supplied by the power generated by the PV modules through a battery system controlled by a battery charger.

Better solutions with active cooling may be obtained using combined systems like PV/T (Photovoltaic Thermal, or Hybrid) solar systems or PV-SAHP (Photovoltaic Solar Assisted Heat Pump) (Gang et al., 2007; Xu et al., 2009; Teo et al., 2012; Rossi et al., 2013; Elnozahya et al., 2015). However, the required temperature levels are not always consistent, so if high temperature heat is needed the PV cell cooling effect will be limited. Other solutions include micro-cooling by using both water and air (Valeh-e-Sheyda et al., 2013).

Direct quantification of the energy consumption to operate the pump or fan for active cooling is generally not indicated. A very small value (44 W h/month) is reported in Elnozahya et al. (2015) for the water spraying system. A few references contain information on the size of the devices. In Salih et al. (2015) the power of the pump for water spraying and circulation is 0.25 Hp (186 W). A centrifugal pump of 1 Hp (746 W) input power is used in Moharram et al. (2013). A DC fan of 6 kW is mentioned in Makki et al. (2015). Exploitation of a 5 kW heat pump is reported in Zhao et al. (2011).

3. Structure of the PV module under study

The performance of the solar cells is typically assessed in dark room by solar simulator at STC, where the mean temperature of the module cells $T_{STC} = 298$ K and the irradiance $G_{STC} = 1000\ W\ m^{-2}$. This equipment simulates a solar spectrum for a short time (<1 s) with Air Mass (AM) equal to 1.5. Very often, in the datasheets of manufacturers, the short circuit current I_{sc}, the current I_{mpp} and the voltage V_{mpp} in Maximum Power Point (MPP) and the open circuit voltage V_{oc} are provided with ±10% tolerance, but the maximum power $P_{max,\ STC}$ (in watt peak, W_p) is guaranteed with ±3% tolerance.

Normally, the manufacturers do not provide the information regarding the thicknesses of the layers which compose the PV module, because they are sensitive data. In the present case, all thicknesses have been provided by the manufacturer. The section of the PV module, sketched in Fig. 1, includes the following layers: (*a*) polycarbonate frontsheet; (*b*) thermoplastic polyurethane (TPU_1); (*c*) 40 series connected m-Si solar cells with an Anti Reflective Coating (ARC), applied on the m-Si solar cells layer in order to reduce sunlight reflection; (*d*) thermoplastic polyurethane (TPU_2); (*e*) a layer made of alveolar polycarbonate ducts, filled with either air (see further Section 4.1.1.) or water (Section 4.1.2); (*f*) an air gap; (*g*) a polycarbonate backsheet.

The 40 solar cells are placed in ten rows made of 4 cells per row; all the cells are series connected. In this application, the coolant fluid is water flowing into the ducts. Due to the presence of the coolant water circulation, the alveolar polycarbonate layer behaves as a heat exchanger. Fig. 2 shows a photo representing the layout of the water cooled PV module and Fig. 3 shows its structure.

The main effects of the cooling system consist of a significant reduction of the operating temperature of the module and the increment of the electrical efficiency.

A second order effect which represents a loss for the system is related to the non-uniformity of the temperature field. In fact, PV modules are made connecting solar cells with current–voltage (I–V) characteristics which should be as similar as possible. If this condition is not respected, as for example in the case of mismatch due to shading or constructive tolerance, the overall module performance may critically drop, due to the presence of different I–V curves (Picault et al., 2010). The amount of losses generated when the cell temperature field is not uniform with a consequent different voltage between the warmer and the cooler cells is investigated in Sections 6 and 7.

4. Theoretical model

The direct measurement of the cell temperature in a PV module is not practical. Indeed, the insertion of a thermal probe is not advisable because it worsens the adhesion of the sheets during the lamination of a PV module. For this reason, a thermal–electrical model is useful to estimate the cell temperatures and the electrical quantities with and without coolant (Spertino et al., 2014). In this model, the cell temperature depends on irradiance and ambient temperature, for negligible wind speeds. In turn, the electrical efficiency is a function of cell temperature.

In this paper, the PV module characterization is given by the thermal model, the electrical model and the determi-

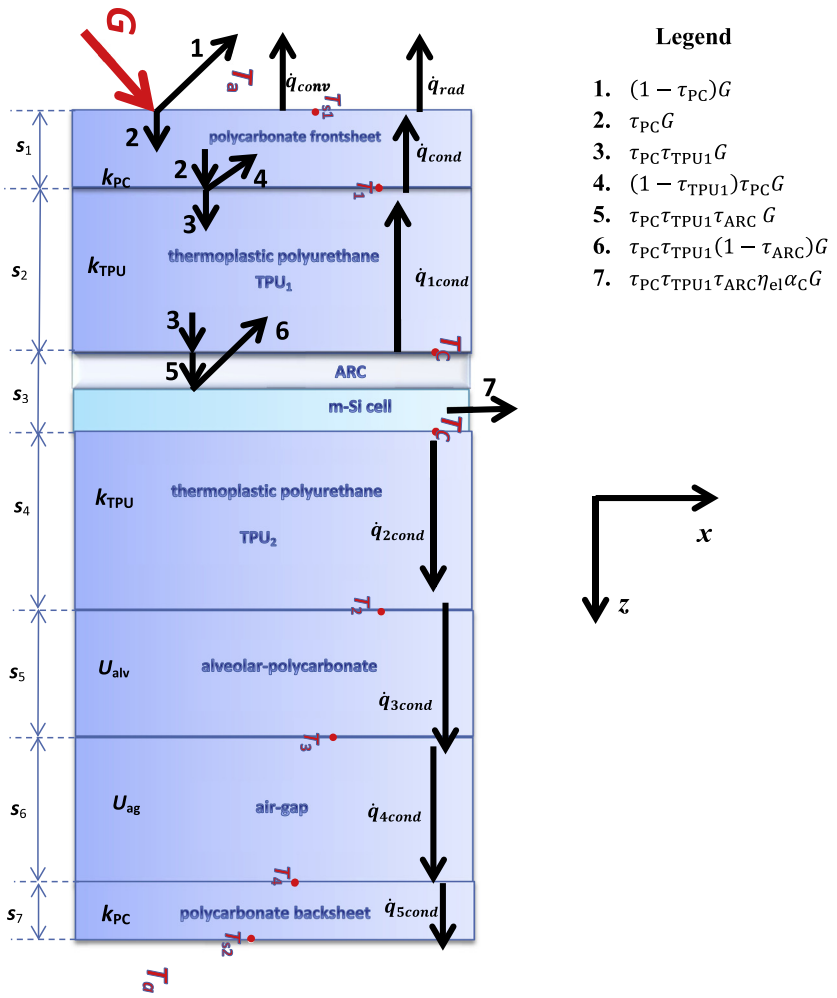

Fig. 1. Structure of the PV module with the different layers without water flow.

nation of its equivalent-circuit parameters, as presented in the following.

4.1. The thermal model

The thermal model is based on computing the heat balance equations in each layer of the PV module, for determining the unknown temperatures at the layer interfaces. The thermal model is analyzed for two cases: PV module without and with water flow and numerical computations are performed in Matlab®.

The PV module can be considered as a multilayer plane wall. The spatial references include: the x and y axes taken on the layers interface surfaces, and the z axis orthogonal to the interface surfaces (Figs. 1 and 4). The values of design parameters are given in Table 1.

4.1.1. PV module without water flow

To analyze the thermal model in this case the following assumptions are considered:

- The heat transfer through the PV module is in steady-state conditions.
- The heat transfer is one-dimensional (1D), since any significant temperature gradients will exist predominantly in the z-direction normal to the PV cell surfaces.
- The thermal conductivities of the layers are constant.
- The thermal contact resistances at the interfaces are negligible.
- The cell thickness is negligible, and the cell temperature T_C is uniform on the cell surface.
- The solar absorptivities α_{TPU} and α_{PC} for the thermoplastic polyurethane (TPU) and polycarbonate (PC) layers are negligible.

The energy balance equation at the interface between ambient and polycarbonate frontsheet is expressed as:

$$\underbrace{\frac{k_{PC}}{s_1}(T_1 - T_{s1})}_{\dot{q}_{cond}} = \underbrace{h_{conv}(T_{s1} - T_a)}_{\dot{q}_{conv}} + \underbrace{\varepsilon\sigma(T_{s1}^4 - T_{sky}^4)}_{\dot{q}_{rad}} \quad (1)$$

where s_1 is the polycarbonate thickness, T_1 is the interface temperature between polycarbonate frontsheet and

Fig. 2. Layout of the PV module with water cooling.

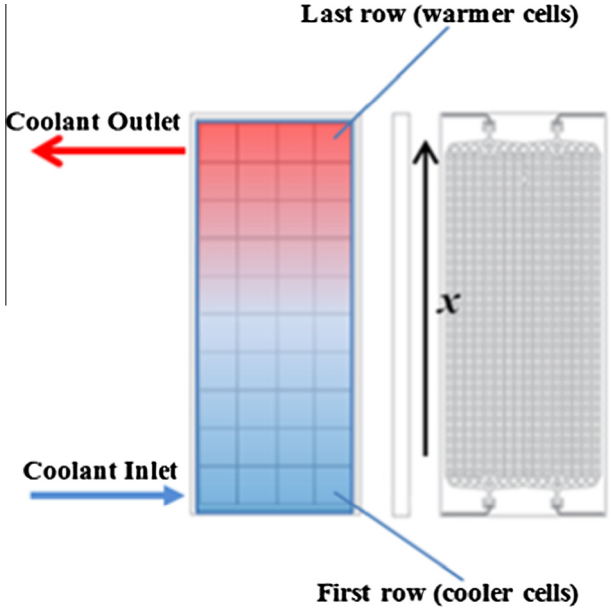

Fig. 3. Sketch of a PV module.

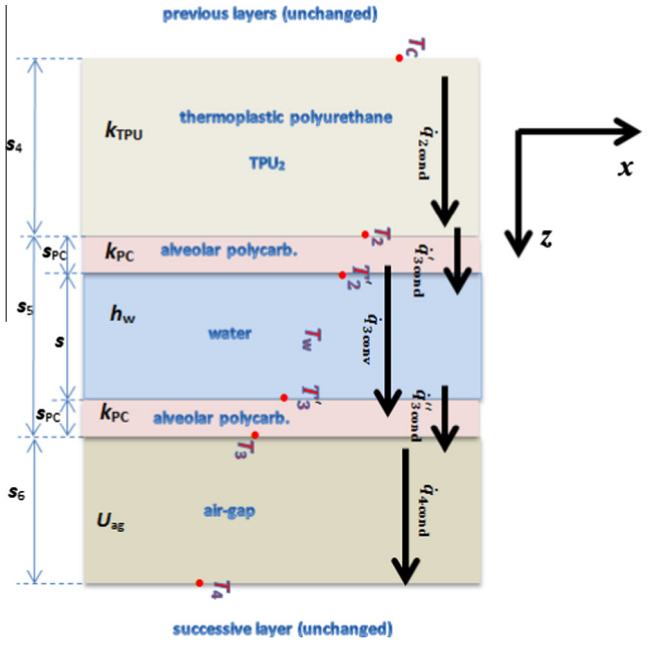

Fig. 4. Structure of the alveolar polycarbonate layer when the water flows.

Table 1
Design parameters used in the thermal model.

Thermal collector design parameters	Value
Conductivity of polycarbonate (PC), k_{PC}	0.2 W m^{-1} K^{-1}
TPU conductivity, k_{TPU}	0.2 W m^{-1} K^{-1}
Thickness of PC front sheet, s_1	0.3750×10^{-3} m
Thickness of the TPU$_1$ sheet, s_2	10^{-3} m
Thickness of the TPU$_2$ sheet, s_4	1.5×10^{-3} m
Thickness of the alveolar polycarbonate layer, s_5	10^{-2} m
Thickness of the polycarbonate sheet, s_{PC}	0.6×10^{-3} m
Thickness of the water duct, s	8.8×10^{-3} m
Air gap thickness, s_6	10^{-2} m
Thickness of the PC backsheet, s_7	4×10^{-3} m
Height of the PV module (water duct), X	1.42 m
Width of the water duct, Y	0.6 m

TPU$_1$, T_{s1} is the polycarbonate frontsheet surface temperature, T_a is the ambient temperature, T_{sky} is the apparent sky temperature, and ε is the polycarbonate emissivity with $0 < \varepsilon < 1$.

Linearization of fourth-power terms in Eq. (1) leads to the well-known expression:

$$T_{s1}^4 - T_{sky}^4 \cong 4T_m^3\left(T_{s1} - T_{sky}\right) \Rightarrow \varepsilon\sigma\left(T_{s1}^4 - T_{sky}^4\right) \cong 4\varepsilon\sigma T_m^3\left(T_{s1} - T_{sky}\right) \cong h_r\left(T_{s1} - T_{sky}\right) \quad (2)$$

where

$$h_r = 4\varepsilon\sigma T_m^3 = 4\varepsilon\sigma \cdot \left[\frac{T_{s1} + T_{sky}}{2}\right]^3 = \varepsilon\sigma\frac{\left(T_{s1} + T_{sky}\right)^3}{2} \quad (3)$$

is the radiative heat transfer coefficient.

By reordering Eq. (1), the energy balance equation at the interface between ambient and polycarbonate frontsheet is written as:

$$\left(h_r + h_{conv} + \frac{k_{PC}}{s_1}\right)T_{s1} - \frac{k_{PC}}{s_1}T_1 = h_r T_{sky} + h_{conv} T_a \quad (4)$$

The apparent sky temperature T_{sky} can be estimated by using the following simplified expression which neglects the atmospheric water vapor pressure (Duffie and Beckman, 1974; ASHRAE, 1999; Bernards, 2004; Notton et al., 2005):

$$T_{sky} = 0.0552 T_a^{1.5} \tag{5}$$

The energy balance equation at the interface between polycarbonate frontsheet and TPU_1 is:

$$\dot{q}_{1,cond} + \tau_{PC} G = \dot{q}_{cond} + \tau_{PC}\tau_{TPU1} G + (1 - \tau_{TPU1})\tau_{PC} G \Rightarrow \underbrace{\frac{k_{TPU}}{s_2}(T_C - T_1)}_{\dot{q}_{1,cond}} = \underbrace{\frac{k_{PC}}{s_1}(T_1 - T_{s1})}_{\dot{q}_{cond}} \tag{6}$$

where G is solar irradiance, s_2 is the TPU_1 thickness, $\dot{q}_{1,cond}$ is the conductive heat flux crossing the TPU_1 sheet, and T_C is the cell temperature inside the module.

By reordering Eq. (5), the energy balance equation at the interface between polycarbonate frontsheet and TPU_1 leads to:

$$\left(\frac{k_{PC}}{s_1} + \frac{k_{TPU}}{s_2}\right) T_1 - \frac{k_{PC}}{s_1} T_{s1} - \frac{k_{TPU}}{s_2} T_C = 0 \tag{7}$$

In the case of the m-Si cell, an Anti Reflective Coating (ARC) placed on the m-Si solar cells layer is considered in order to reduce sunlight reflection. Furthermore, the cell is an opaque surface and the solar absorptivity of cell is considered $\alpha_C \cong 1$. Part of the global irradiance is converted into electrical power and another part is transformed into heat, leading to the increase of the cell temperature T_C. Consequently, the energy balance equation for m-Si solar cell of PV module is given by:

$$\tau_{PC}\tau_{TPU1}\tau_{ARC}(1-\eta_{el})\alpha_C G = \tau_{PC}\tau_{TPU1}(1-\tau_{ARC})G + \underbrace{\frac{k_{TPU}}{s_2}(T_C - T_1)}_{\dot{q}_{1,cond}} + \underbrace{\frac{k_{TPU}}{s_4}(T_C - T_2)}_{\dot{q}_{2,cond}} \tag{8}$$

where η_{el} is the PV cell electrical efficiency, τ_{ARC} is the ARC transmissivity, $\tau_{PC}\tau_{TPU1}\tau_{ARC}\eta_{el}\alpha_C G$ is the fraction of global irradiance converted into electrical power, $\dot{q}_{2,cond}$ is the conductive heat transfer flux crossing the TPU_2 sheet, s_4 is the TPU_2 thickness, and T_2 is the interface temperature between the TPU_2 sheet and alveolar polycarbonate layer.

By reordering Eq. (8), the energy balance equation at the m-Si solar cell of PV module leads to:

$$\left(\frac{k_{TPU}}{s_2} + \frac{k_{TPU}}{s_4}\right) T_C - \frac{k_{TPU}}{s_2} T_1 - \frac{k_{TPU}}{s_4} T_2 = [(2 - \eta_{el})\tau_{ARC} - 1]\tau_{PC}\tau_{TPU1} G \tag{9}$$

This heat balance equation, therefore, requires the knowledge of the electrical efficiency η_{el}, which is calculated by the electrical model in Section 4.2.

Since the m-Si cell surface is opaque to solar radiation, all thermal fluxes crossing the surfaces below the cell are conductive heat transfer fluxes. The only exception is on the interface between polycarbonate backsheet and environment, where convective and radiative heat fluxes are additionally involved.

The energy balance equation at the interface between TPU_2 and alveolar polycarbonate layer is:

$$\underbrace{\frac{k_{TPU}}{s_4}(T_C - T_2)}_{\dot{q}_{2,cond}} = \underbrace{U_{alv}(T_2 - T_3)}_{\dot{q}_{3,cond}} \Rightarrow \left(U_{alv} + \frac{k_{TPU}}{s_4}\right) T_2 - \frac{k_{TPU}}{s_4} T_C - U_{alv} T_3 = 0 \tag{10}$$

where T_3 is the interface temperature between the alveolar polycarbonate layer and air–gap, U_{alv} is the overall heat transfer coefficient in the alveolar polycarbonate layer, $\dot{q}_{3,cond}$ is the conductive heat transfer flux crossing the alveolar polycarbonate layer.

In the ducts of the alveolar polycarbonate layer, for the present case, there is no water flowing inside the ducts, but still air. Due to its small thickness ($s_5 = 0.0006$ m) the polycarbonate sheet thermal resistance can be neglected with respect to the air gap whose overall heat transfer coefficient is estimated by the following expression (Holman, 2010):

$$U_{alv} = 1.42 \cdot \left(\frac{T_2 - T_3}{2Y \sin\beta}\right)^{0.25} + 4 \cdot \frac{1}{\frac{1}{\varepsilon_1} + \frac{1}{\varepsilon_2} - 1} \sigma \cdot \left(\frac{T_2 + T_3}{2}\right)^3 \tag{11}$$

where β is the tilt angle of the PV module, Y is the width of the PV module, ε_1, ε_2 are the alveolar polycarbonate layer emissivity values approximated as $\varepsilon_1 = \varepsilon_2 \cong 0.9$. The resulting overall heat transfer coefficient is $U_{alv} \cong 6\ W\ m^{-2}\ K^{-1}$.

The energy balance equation at the interface between alveolar polycarbonate layer and air–gap layer is given by:

$$\underbrace{U_{alv}(T_2 - T_3)}_{\dot{q}_{3,cond}} = \underbrace{U_{ag}(T_3 - T_4)}_{\dot{q}_{4,cond}} \Rightarrow (U_{ag} + U_{alv})T_3 - U_{alv} T_2 - U_{ag} T_4 = 0 \tag{12}$$

where U_{ag} is the overall heat transfer coefficient in the air–gap layer, T_4 is the interface temperature between the air–gap layer and polycarbonate backsheet, and $\dot{q}_{4,cond}$ is the conductive heat transfer flux crossing the air–gap layer.

The overall heat transfer coefficient in the air–gap layer U_{ag} is estimated with the same Eq. (11) expression as for U_{alv}:

$$U_{ag} = 1.42 \cdot \left(\frac{T_3 - T_4}{2Y \sin\beta}\right)^{0.25} + 4 \cdot \frac{1}{\frac{1}{\varepsilon_3} + \frac{1}{\varepsilon_4} - 1} \sigma \cdot \left(\frac{T_3 + T_4}{2}\right)^3 \tag{13}$$

where the air–gap layer emissivity values are approximated as $\varepsilon_3 = \varepsilon_4 \cong 0.9$.

The energy balance equation at the interface between air–gap layer and polycarbonate backsheet is given by:

$$\underbrace{U_{ag}(T_3 - T_4)}_{\dot{q}_{4,cond}} = \underbrace{\frac{k_{PC}}{s_7}(T_4 - T_{s2})}_{\dot{q}_{5,cond}} \Rightarrow \left(U_{ag} + \frac{k_{PC}}{s_7}\right) T_4 - \frac{k_{PC}}{s_7} T_{s2} - U_{ag} T_3 = 0 \quad (14)$$

where $\dot{q}_{5,cond}$ is the conductive heat transfer flux crossing the polycarbonate backsheet, T_{s2} is the polycarbonate backsheet surface temperature, and s_7 is the polycarbonate backsheet thickness.

The energy balance equation at the interface between polycarbonate backsheet and environment is given by:

$$\underbrace{\frac{k_7}{s_7}(T_4 - T_{s2})}_{\dot{q}_{5,cond}} = \underbrace{h_{conv}(T_{s2} - T_a)}_{\dot{q}_{1,conv}} + \underbrace{\varepsilon\sigma(T_{s2}^4 - T_{sky}^4)}_{\dot{q}_{1,rad}} \quad (15)$$

where $\dot{q}_{1,conv}$ and $\dot{q}_{1,rad}$ the convective and radiative heat fluxes from polycarbonate backsheet to environment.

The term T_{s2}^4 in Eq. (14) is linearized by means of the same expression used in Eq. (3):

$$T_{s2}^4 - T_{sky}^4 \cong 4T_m^3(T_{s2} - T_{sky}) \Rightarrow \varepsilon\sigma(T_{s2}^4 - T_{sky}^4) \cong 4\varepsilon\sigma T_m^3(T_{s2} - T_{sky}) \cong h_{r1}(T_{s2} - T_{sky}) \quad (16)$$

where

$$h_{r1} = 4\varepsilon\sigma T_m^3 = 4\varepsilon\sigma \cdot \left[\frac{T_{s2} + T_{sky}}{2}\right]^3 = \varepsilon\sigma \frac{(T_{s2} + T_{sky})^3}{2} \quad (17)$$

By reordering Eq. (14), the energy balance equation at the interface between polycarbonate backsheet and environment is written as:

$$\left(h_{r1} + h_{conv} + \frac{k_{PC}}{s_7}\right) T_{s2} - \frac{k_{PC}}{s_7} T_4 = h_{r1} T_{sky} + h_{conv} T_a \quad (18)$$

The seven unknown temperatures are contained in the vector $\mathbf{x} = [T_{s1},\ T_1,\ T_C,\ T_2,\ T_3,\ T_4,\ T_{s2}]^T$, for the linear system solution, where the superscript T denotes transposition.

To calculate the unknowns, a linear system of equations is obtained in the form $\mathbf{A} \cdot \mathbf{x} = \mathbf{b}$ (see Appendix A.1).

Since the terms h_r, U_{alv}, U_{ag} and h_{r1} depend on some unknown temperatures, the unknowns cannot be found in a single solution of the linear system $\mathbf{A} \cdot \mathbf{x} = \mathbf{b}$. Therefore, an iterative process is needed. Initial values are set up for h_r, U_{alv}, U_{ag} and h_{r1} and the unknown vector $\mathbf{x}$ is calculated by solving the linear system $\mathbf{A} \cdot \mathbf{x} = \mathbf{b}$. After that, the values of h_r, U_{alv}, U_{ag} and h_{r1} are recalculated by using Eqs. (3), (11), (13) and (17), respectively. This process is iteratively repeated until the errors on variables U_{ag} and h_{r1} become lower than a specified tolerance. After convergence, all the unknown temperatures are found.

4.1.2. PV module with water flow

In this case, there is water flowing in the alveolar polycarbonate layer. The water temperature T_w increases along the space variable x which represents the water flow direction. The basic assumptions are the same as in the PV module without water flow, the only difference being in the alveolar polycarbonate layer, where the water flows. In this layer, it is assumed that the water temperature T_w depends only on the space variable x.

When water flows, the alveolar polycarbonate previously considered as one single slab is now modeled as three different layers. Two layers are made of polycarbonate sheets. The third one is an intermediate gap where the water flows (Fig. 4).

The energy balance equations remain unchanged as in the case with PV module without water flow. The only exceptions for these equations refer to the following five interfaces:

(i) *The interface between TPU_2 and the first sheet of alveolar polycarbonate:* the energy balance equation at the interface between TPU_2 and first alveolar polycarbonate layer is

$$\underbrace{\frac{k_{TPU}}{s_4}(T_C - T_2)}_{\dot{q}_{2,cond}} = \underbrace{\frac{k_{PC}}{s_{PC}}(T_2 - T_2')}_{\dot{q}_{3',cond}} \Rightarrow \left(\frac{k_{TPU}}{s_4} + \frac{k_{PC}}{s_{PC}}\right) T_2 - \frac{k_{TPU}}{s_4} T_c - \frac{k_{PC}}{s_{PC}} T_2' = 0 \quad (19)$$

where $\dot{q}_{3',cond}$ is the conductive heat transfer flux crossing first alveolar polycarbonate layer, T_2' is the first new unknown temperature at the interface between the polycarbonate sheet and the water layer, and s_p is the thickness of the first polycarbonate sheet itself.

(ii) *The interface between the first sheet of alveolar polycarbonate and the water layer*: the energy balance equation at the interface between the first polycarbonate sheet and the water layer is

$$\frac{k_{PC}}{s_{PC}}(T_2 - T_2') = h_w(T_2' - T_w) \Rightarrow \left(\frac{k_{PC}}{s_{PC}} + h_A\right) T_2' - \frac{k_{PC}}{s_{PC}} T_2 = h_w T_w \quad (20)$$

where h_w is the water heat convective coefficient. The coefficient h_w is evaluated after computing the Nusselt number Nu, which has been considered fixed for a laminar flow (low Reynolds number, as shown in Table 2) in square ducts at the value Nu = 3.608 (Lienhard and Lienhard, 2015). The Reynolds number is $Re = \frac{\bar{w} \cdot d_h}{\nu_w}$, where $\bar{w} = \dot{v} \cdot s \cdot Y$ the mean velocity of water is, $\dot{v}$ is the volume flow rate of water, and ν_w is the kinematic viscosity of water.

Hence, considering the hydraulic diameter of water flows passage d_h, and the water thermal conductivity k_w:

$$h_w = Nu k_w d_h^{-1} \quad (21)$$

The hydraulic diameter d_h depends on the cross-sectional area $A_c = s \cdot Y$ and on the perimeter

$p = 2(s + Y)$ of the duct (Fig. 5) and is given by:

$$d_h = 4A_c \cdot p^{-1} \Rightarrow d_h = 2s \cdot Y \cdot (s + Y)^{-1} \quad (22)$$

where Y is the dimension along y direction of the alveolar polycarbonate layer (equal to the width of the PV module).The water properties (density ρ_w, thermal conductivity k_w, kinematic viscosity ν_w, and specific heat c) are evaluated at the bulk mean water temperature. This temperature represents the arithmetic average of the mean water temperatures at the inlet and outlet of the duct: $T_b = \frac{T_{w,in}+T_{w,out}}{2}$ (Çengel and Turner, 2001).

(iii) *Inside the water layer which behaves as a heat exchanger*: the energy balance inside the water layer is given by an equation similar to a heat exchanger energy balance (Fig. 5):

$$\underbrace{h_w(T'_2 - T_w)}_{\dot{q}_{3'conv}} \underbrace{Y \cdot dx}_{dA} = \dot{v} \cdot c \cdot dT_w + \underbrace{h_w(T_w - T'_3)}_{\dot{q}_{3''conv}} \underbrace{Y \cdot dx}_{dA} \quad (23)$$

where $\dot{q}_{3',conv}$ is the convective heat transfer flux from first alveolar polycarbonate layer to the water, $\dot{q}_{3'',conv}$ is the convective heat transfer flux from the water to the second alveolar polycarbonate layer, $\dot{v}$ is the volume flow rate of water, c is the specific heat of water, dA is the infinitesimal surface element of heat transfer. Reordering Eq. (23) the energy balance equation inside the water layer is:

$$\frac{\dot{v} \cdot c}{Y}\frac{dT_w}{dx} - T'_2 h_w - T'_3 h_w = -2T_w h_w$$
$$\Rightarrow \frac{\dot{v} \cdot c}{Y} Z - T'_2 h_w - T'_3 h_w = -2T_w h_w \quad (24)$$

where $Z = \frac{dT_w}{dx}$ is the x-dimension derivative of the water temperature, considered as a new unknown term.

(iv) *The interface between the water layer and the second sheet of alveolar polycarbonate:* the energy balance equation at the interface between the water layer and the second alveolar polycarbonate layer:

$$h_w(T_w - T'_3) = \underbrace{\frac{k_{PC}}{s_{PC}}(T'_3 - T_3)}_{\dot{q}_{3'',cond}} \Rightarrow \left(\frac{k_{PC}}{s_{PC}} + h_A\right) T'_3$$
$$- \frac{k_{PC}}{s_{PC}} T_3 = h_w T_w \quad (25)$$

where $\dot{q}_{3',cond}$ is the conductive heat transfer flux crossing the second alveolar polycarbonate layer

Table 2
Water parameters used in the thermal model.

T_w (K)	k_w (W m^{-1} K^{-1})	ν_w (m^2 s^{-1})	Re	h_w (W m^{-2} K^{-1})
288	0.5892	1.157×10^{-6}	13.64	241.57
293	0.5984	1.006×10^{-6}	15.69	245.34
313	0.6305	0.658×10^{-6}	23.98	258.50
333	0.6543	0.475×10^{-6}	33.22	268.26

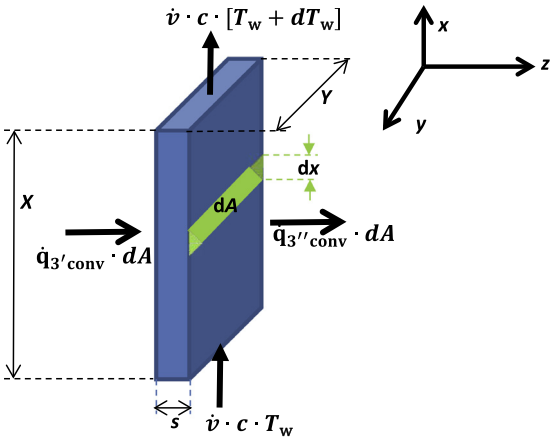

Fig. 5. Heat energy balance for the water layer.

and T'_3 is the temperature at the interface between the second polycarbonate sheet and the water layer.

(v) *The interface between the second sheet of alveolar polycarbonate and the air gap*: the balance equation at the interface between the second polycarbonate sheet and the air gap:

$$\frac{k_{PC}}{s_{PC}}(T'_3 - T_3) = U_{ag}(T_3 - T_4) \Rightarrow \left(U_{ag} + \frac{k_{PC}}{s_{PC}}\right) T_3$$
$$- U_{ag} T_4 - \frac{k_{PC}}{s_{PC}} T'_3 = 0 \quad (26)$$

Now, there are ten unknowns in the vector $\mathbf{x}_Z = [T_{s1}, T_1, T_C, T_2, T'_2, Z, T'_3, T_3, T_4, T_{s2}]^T$ including nine temperatures and the term Z. The spatial domain is discretized by defining the elementary step $dx = x_{n+1} - x_n$, where the step counter n starts from zero and terminates when $x_n = X–dx$. The derivative Z is discretized by using finite differences as:

$$Z = \frac{T_w(x_{n+1}) - T_w(x_n)}{dx} \quad (27)$$

To calculate the unknowns, a linear system of equations is obtained in the form $\mathbf{A}_Z \cdot \mathbf{x}_Z = \mathbf{b}_Z$ (see Appendix A.2).

The procedure to obtain the numerical solution is set up as follows, starting from $n = 0$ with $T_w(x_0) = T_{w,in}$, being $T_{w,in}$ the water temperature at the alveolar polycarbonate layer input:

1. Solve the linear system of equations $\mathbf{A}_Z \cdot \mathbf{x}_Z = \mathbf{b}_Z$, from which the derivative Z is obtained among the other unknowns.
2. Calculate x_{n+1} from (27):

$$T_w(x_{n+1}) = T_w(x_n) + Z \cdot dx \quad (28)$$

3. Repeat the calculations until $x_n = X - dx$.

Again, the terms h_r, U_{alv}, U_{ag} and h_{r1} depend on some unknown temperatures. Hence, an iterative process is run as in the case without water discussed in Section 4.1.1. However, now the temperatures depend on the spatial

variable x. Thereby, the iterative process has to be repeated for each step dx along the x-dimension.

4.2. The electrical model

The electrical model presented in this paper is based on the junction described by a single exponential in order to simulate the I–V characteristics of the PV module (Liu and Dougal, 2002; Xiao et al., 2004; Villalva et al., 2009; Ayedh et al., 2012; Andrei et al., 2013; Bellia et al., 2014). The one-diode model of a solar cell consists of five parameters: a current source representing the photo-generated current I_{ph}, a diode with two parameters ($-I_0$ and m), and two resistances (series R_{ser} and parallel R_{sh}), as depicted in Fig. 6. The Shockley diode equation is expressed as follows (Villalva et al., 2009):

$$I_D = I_0\left[\exp\left(\frac{V_D}{V_t}\right) - 1\right] \Rightarrow I_D = I_0\left[\exp\left(\frac{q \cdot V_D}{m \cdot \kappa \cdot T_C}\right) - 1\right] \quad (29)$$

where I_D is the diode current, $-I_0$ is the diode reverse saturation current (strongly dependent on the cell temperature T_C and with negative sign to indicate a reverse bias), V_D is the diode voltage, V_t is thermal voltage of the diode related to T_C, $q = 1.60217646 \cdot 10^{-19}$ C is the electron charge, m is the diode ideality factor, and $\kappa = 1.3806503 \cdot 10^{-23}$ J K^{-1} is the Boltzmann constant.

The fundamental equations, obtained from the Kirchhoff's laws, for the solar cell, are presented below (Rauschenbach, 1980; Park and Yu, 2004; Villalva et al., 2009; Chatterjee and Keyhani, 2011):

$$V = V_D - R_{ser}I \Rightarrow V_D = V + R_{ser}I \quad (30)$$

$$I = I_{ph} - I_D - \frac{V_D}{R_{sh}} \Rightarrow I = I_{ph} - I_0\left[\exp\left(\frac{q \cdot V_D}{m \cdot \kappa \cdot T_C}\right) - 1\right] - \frac{V + R_{ser}I}{R_{sh}} \quad (31)$$

where V is the output voltage, I is the output current, I_{ph} is the photo-generated current, R_{ser} and R_{sh} are the series resistance and the shunt resistance, respectively.

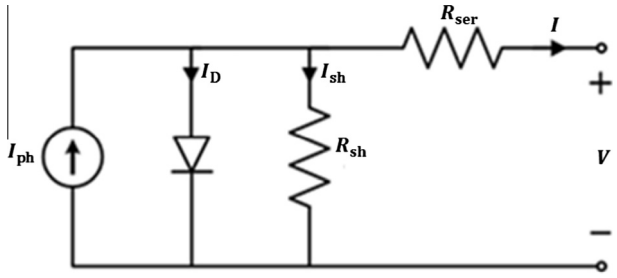

Fig. 6. Equivalent circuit of solar cell with one-diode model.

Usually, this system of equations describes the PV cell behavior at STC. In common applications, the manufacturer provides the three typical points of the I–V curve and their thermal coefficients. They are the short circuit current I_{sc}, the open-circuit voltage V_{oc} and the maximum power $P_{max,STC}$ with the corresponding thermal coefficients α_{Isc}, β_{Voc} and γ_P (in this case is about 0.0045 °C^{-1}). One of the goals of this work is to build a full theoretical model without these coefficients strictly related to a particular PV technology. The electrical efficiency η_{el} varies linearly with temperature and is given by the following expression (Florschuetz, 1975; Evans, 1981; Ben Cheikh el Hocine et al., 2015):

$$\eta_{el} = \underbrace{\frac{P_{max,STC}}{G_{STC} \cdot A_{PVm}}}_{\eta_{el,STC}} \cdot [1 - \gamma_P \cdot (T_C - T_{STC})] \Rightarrow \eta_{el} = \frac{P_{max}}{G \cdot A_{PVm}} = \eta_{el,STC} \cdot [1 - 0.0045 \cdot (T_C - T_{STC})] \quad (32)$$

where $\eta_{el,STC}$ is the electrical efficiency at STC in per unit, and A_{PVm} is the total area of the PV module.

This is a simple solution to obtain a full electrical model, but the five parameters of the equivalent circuit are not provided by the manufacturer. Thus, a procedure to derive these parameters is explained in Section 4.2.1. These equations allow calculating the I–V curve in every irradiance and temperature conditions. Regarding the current source, it depends on the structure of the solar cells (Tiwari and Dubey, 2010) and on the spectral irradiance and temperature (Moballegh and Jiang, 2011). The photo-generated current I_{ph} is proportional to the cell surface S_C and is a non-linear function of the solar spectrum $\Phi(\lambda)$ with respect to the wavelength λ (Pierro et al., 2015). This non-linear function is the spectral response of the solar cell $SR(\lambda)$ according to the following formula:

$$I_{ph} = S_C \cdot \int_\lambda SR(\lambda) \cdot \Phi(\lambda) d\lambda \quad (33)$$

To simplify the above mentioned dependence on the solar spectrum, the spectral-response parameter K_{ph} is Martín and Ruiz (1999):

$$I_{ph} = S_C \cdot \underbrace{\frac{\int_\lambda SR(\lambda) \cdot \Phi(\lambda) d\lambda}{\int_\lambda \Phi(\lambda) d\lambda}}_{K_{ph}} \cdot \underbrace{\int_\lambda \Phi(\lambda) d\lambda}_{G} \Rightarrow I_{ph} = S_C \cdot K_{ph} \cdot G \quad (34)$$

where the irradiance G is the integral of the solar spectrum. Some expressions to represent the dependence of I_0, I_{ph} and energy gap E_G in one-diode model on cell temperature are indicated below (Lasnier and Ang, 1990; Patel, 1999; Walker, 2001; Messenger and Ventre, 2004; De Soto et al., 2006; Villalva et al., 2009; Farivar and Asaei, 2010; Attivissimo et al., 2013; Siddique et al., 2013):

$$I_0 = I_{0,\mathrm{STC}}\left(\frac{T_\mathrm{C}}{T_\mathrm{STC}}\right)^3 \times \exp\left(-\frac{E_\mathrm{G}}{\kappa \cdot T_\mathrm{C}}\right)\Big/ \exp\left(-\frac{E_\mathrm{G}}{\kappa \cdot T_\mathrm{STC}}\right) \quad (35)$$

$$I_\mathrm{ph} = I_{\mathrm{ph,STC}}\frac{G}{G_\mathrm{STC}}[1 + \alpha_{Isc}(T_\mathrm{C} - T_\mathrm{STC})] \quad (36)$$

$$E_\mathrm{G} = E_{\mathrm{G0}} - \frac{\varphi T_\mathrm{C}^2}{T_\mathrm{C} + \psi} \quad (37)$$

where $I_{0,\mathrm{STC}}$ is the diode saturation current at STC conditions (this can be evaluated by referring to the open circuit condition), $I_{\mathrm{ph,STC}}$ is the photo current at STC, G_STC is the irradiance at STC, α_Isc is the short circuit current coefficient, T_STC is the temperature at STC, E_G is the energy gap of the cell at temperature T_C, E_{G0} the energy gap at absolute zero (for crystalline silicon cells $E_{\mathrm{G0}} = 1.21$ eV), φ and ψ are constants depending on the cell material. In conclusion, the electrical model developed requires only one empirical coefficient α_Isc, while the maximum power coefficient and the open circuit coefficient are not required.

4.2.1. Determination of the equivalent-circuit parameters

As above mentioned, manufacturers usually do not provide the five parameters of cell equivalent circuit, but declares three meaningful points on the I–V curve at STC (Xiao et al., 2004; Chatterjee and Keyhani, 2011). These are the short circuit, open circuit, and MPP (Villalva et al., 2009). The five unknown parameters are determined starting from the information referring to I_sc, V_mpp, I_mpp and V_oc (Nayak et al., 2013; Shongwe, 2015). In open circuit conditions, with $I = 0$ and $V_\mathrm{D} = V_\mathrm{oc}$ in Eq. (31), replacing $I_{\mathrm{ph,STC}} = S_\mathrm{C}K_\mathrm{ph}G_\mathrm{STC}$, the current balance yields:

$$I_{\mathrm{ph,STC}} - \frac{V_\mathrm{oc}}{R_\mathrm{sh}} = I_{0,\mathrm{STC}} \cdot \left[\exp\left(\frac{qV_\mathrm{oc}}{m\kappa T_\mathrm{STC}}\right) - 1\right] \Rightarrow I_{0,\mathrm{STC}} = \frac{G_\mathrm{STC}K_\mathrm{ph}S_\mathrm{C} - \frac{V_\mathrm{oc}}{R_\mathrm{sh}}}{\exp\left(\frac{qV_\mathrm{oc}}{m\kappa T_\mathrm{STC}}\right) - 1} \quad (38)$$

Through Eq. (38) the saturation current $I_{0,\mathrm{STC}}$ is determined. In short circuit conditions, with $I = I_\mathrm{sc}$ and $V = 0$ in Eq. (31), and with $V_\mathrm{D} = R_\mathrm{ser}I_\mathrm{sc}$, the following equation is obtained:

$$I_\mathrm{sc} = I_\mathrm{ph} - I_\mathrm{D} - \frac{R_\mathrm{ser}}{R_\mathrm{sh}}I_\mathrm{sc} = I_\mathrm{ph} - I_{0,\mathrm{STC}}\left[\exp\left(\frac{qR_\mathrm{ser}I_\mathrm{sc}}{m\kappa T}\right) - 1\right] - \frac{R_\mathrm{ser}}{R_\mathrm{sh}}I_\mathrm{sc} \quad (39)$$

Eq. (39) can be approximated by considering that in short circuit conditions the current I_D can be neglected, being the voltage at the diode terminals lower than the cut-in voltage (Millman and Grabel, 1987). Thereby, Eq. (39) becomes:

$$I_\mathrm{ph} - \frac{R_\mathrm{ser} + R_\mathrm{sh}}{R_\mathrm{sh}}I_\mathrm{sc} = 0 \quad (40)$$

In MPP, $I = I_\mathrm{mpp}$ and $V = V_\mathrm{mpp}$, the next equation is obtained from Eqs. (29)–(31):

$$\left(-\frac{R_\mathrm{ser}}{R_\mathrm{sh}} - 1\right)I_\mathrm{m} - \frac{V_\mathrm{m}}{R_\mathrm{sh}} + G_\mathrm{STC}K_\mathrm{ph}S_\mathrm{C} - I_{0,\mathrm{STC}}\left\{\exp\left[\frac{q}{m\kappa T_\mathrm{STC}}(V_\mathrm{m} + R_\mathrm{ser}I_\mathrm{m}) - 1\right]\right\} = 0 \quad (41)$$

Eqs. (40) and (41) form a nonlinear system of two equations, with the four unknowns K_ph, m, R_ser and R_sh. Since R_sh is generally some orders of magnitude higher than R_ser, a fixed value has been set up for $R_\mathrm{sh} = 200\ \Omega$, to make negligible the current inside the shunt resistance. The number of unknowns is, then, reduced to three. The acceptable ranges of variation for the parameters (Karatepe et al., 2007) are $m \in [1, 2]$, $K_\mathrm{ph} \in [0.3, 0.4]$ (from manufacturers of solar cells: e.g., bSolar GmbH, 2015), and R_ser around a few m Ω. The solution of the model is based on the minimization of the quadratic function given by the sum of the squares of Eqs. (40) and (41), that is:

$$\mathrm{Min}_{K_\mathrm{ph},m,R_\mathrm{ser}}\left\{\left[\left(-\frac{R_\mathrm{ser}}{R_\mathrm{sh}} - 1\right)I_\mathrm{m} - \frac{V_\mathrm{m}}{R_\mathrm{sh}} + G_\mathrm{STC}K_\mathrm{ph}S_\mathrm{C} - \frac{G_\mathrm{STC}K_\mathrm{ph}S_\mathrm{C} - \frac{V_\mathrm{oc}}{R_\mathrm{sh}}}{\exp\left(\frac{qV_\mathrm{oc}}{m\kappa T_\mathrm{STC}}\right) - 1}\left(\exp\left(\frac{q}{m\kappa T_\mathrm{STC}}(V_\mathrm{m} + R_\mathrm{ser}I_\mathrm{m}) - 1\right)\right)\right]^2 + \left[G_\mathrm{STC}K_\mathrm{ph}S_\mathrm{C} - \frac{R_\mathrm{ser} + R_\mathrm{sh}}{R_\mathrm{sh}}I_\mathrm{sc}\right]^2\right\} \quad (42)$$

The solution shown in Table 3 is calculated with the function *fmincon* (Matlab®) that searches the minimum of a constrained function by assuming that the variables change within specified limits, by using the trust-region-reflective algorithm (Coleman and Li, 1996).

This minimization procedure has been tested by using different PV module datasheets, obtaining excellent agreement between the meaningful points provided by manufacturer and the three points calculated on the I–V curves. For this reason, the thermal–electric model can be adopted to verify the declared electrical data as explained in Section 6.

5. Application of thermal–electrical model to calculate the temperature and performance of solar cell

The procedure regarding the thermal–electric model for obtaining the cell temperature T_C and the I–V curves at different conditions of solar irradiance and ambient temperature (G, T_a) is represented in Fig. 7. The iterative procedure consists of two steps which are mutually linked as in a feedback loop.

I. The *Thermal model* block calculates the initial cell temperature value T_C, with the STC efficiency $\eta_{\mathrm{el,STC}}$, provided by either the manufacturer or the outdoor experimental testing. Other fundamental

Table 3
Electrical parameter of the PV module.

Electrical parameter	Value
R_{sh} (Ω)	200
R_{ser} (Ω)	7.64×10^{-3}
m	1.249
$I_{ph,STC}$ (A)	4.73
$I_{0,STC}$ (A)	9.2×10^{-8}
α_{Isc} (%/°C)	0.038

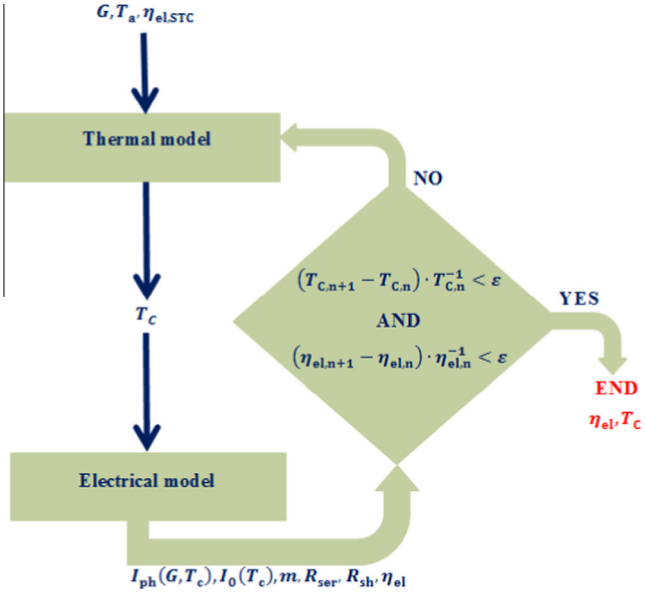

Fig. 7. Scheme of the complete thermal–electrical procedure.

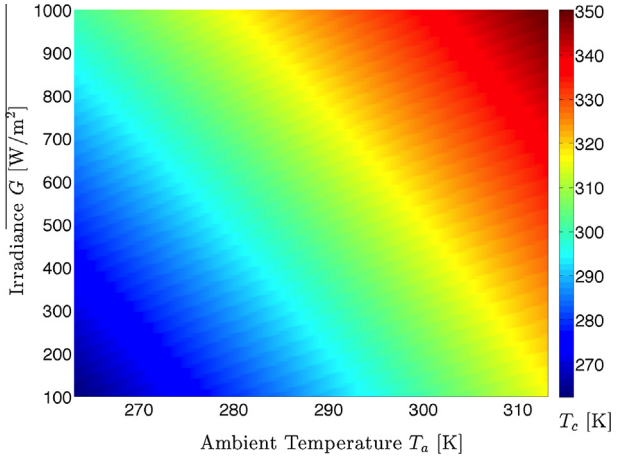

Fig. 8. Cell temperature calculated by the thermal–electrical model (without cooling).

data for starting the procedure are solar irradiance, ambient temperature, and the coolant parameters (water flow-rate and its temperature).

II. the *Electrical model* block calculates the theoretical cell parameters starting from the STC data; using the final cell temperature T_C, the same block determines the corrected efficiency η_{el} by which it is possible to calculate the I–V curves in whatever ambient condition.

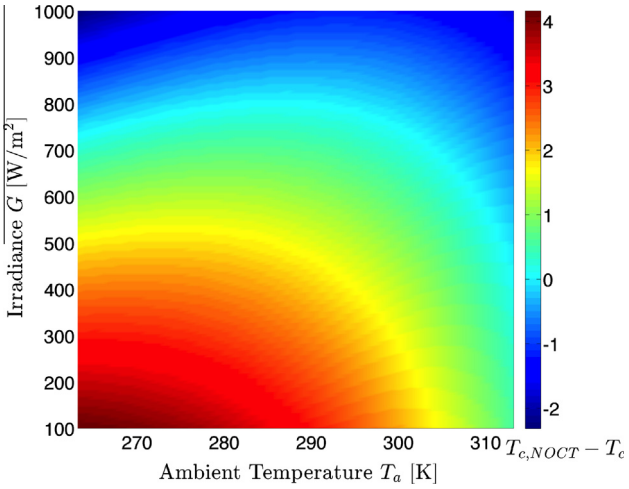

Fig. 9. Temperature differences calculated between NOCT approach and thermal–electrical model (without cooling).

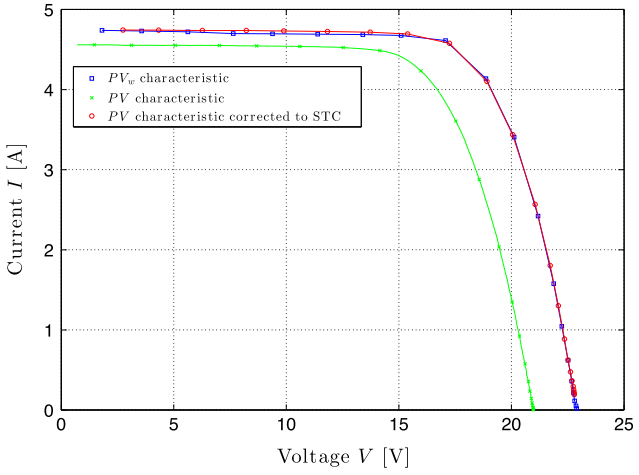

Fig. 10. Experimental I–V curves without cooling before/after correction to STC and I–V curve with water cooling.

At iteration $n + 1$, the cell temperature and the electrical efficiency are compared with the previous values; if the relative differences exceed a suitable fixed tolerance (10^{-5}), the iterative procedure continues; otherwise, the iterative procedure stops.

The theoretical model is developed either with or without coolant flow. In the absence of coolant flow, it is interesting to compare the cell temperature calculated by using this model with the cell temperature calculated by an empirical formula which involves a certification parameter called the NOCT (Nominal Operating Cell Temperature, IEC 61215, 2005). NOCT, reported in the PV module datasheets, is obtained from outdoor measurements by a thermal probe placed on the rear side of the PV module mounted on an open structure. It is the temperature

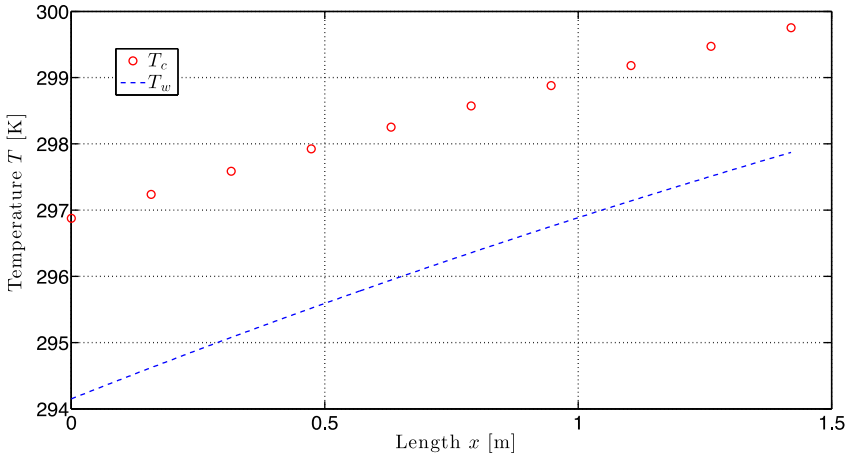

Fig. 11. Cell and coolant temperature profiles by the thermal model (ten rows made of 4 solar cells).

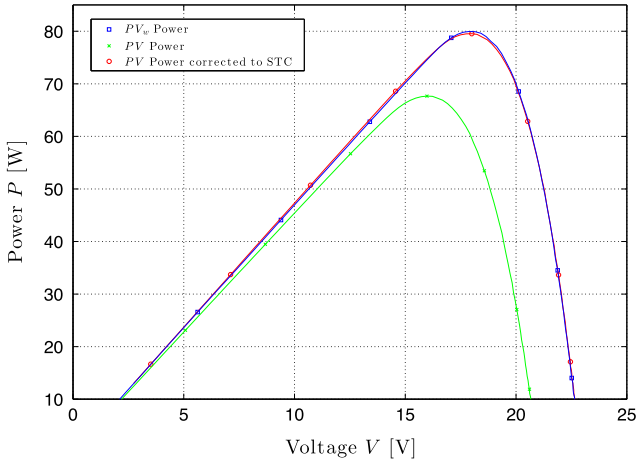

Fig. 12. Experimental P–V curves without cooling before/after correction to STC and P–V curve with water cooling.

Table 4
STC electrical data of the PV module.

Electrical parameter	Estimated value	Declared value
I_{sc} (A)	4.75	4.83
U_{oc} (V)	22.86	24.01
I_{max} (A)	4.46	4.48
U_{max} (V)	17.94	19.57
P_{max} (W)	80.01	87.61

reached by the backsheet of the module in open circuit, under the following conditions: solar irradiance $G = 800\ \mathrm{W\,m^{-2}}$, ambient temperature $T_a = 20\ ^\circ\mathrm{C}$, and wind speed $w_a = 1\ \mathrm{m\,s^{-1}}$.

This empirical formula states a linear dependence between the solar irradiance and the difference between the cell temperature and ambient temperature (Nolay, 1987; Lasnier and Ang, 1990; ASTM, 1998; Myers et al., 2002):

$$T_C = T_a + \frac{\mathrm{NOCT} - 20}{800} \cdot G \tag{43}$$

The cell temperatures, calculated through the theoretical model at different conditions of irradiance and ambient temperature (G, T_a), are reported in Fig. 8. The difference between the theoretical model and the empirical formula (43) is displayed in Fig. 9: it exhibits a good agreement. The maximum difference is within $(-2\ \mathrm{K},\ +4\ \mathrm{K})$ in the ranges $G = 100$–$1000\ \mathrm{W\,m^{-2}}$ and $T_a = 0$–$40\ ^\circ\mathrm{C}$.

6. Adjustment of parameters in the thermal–electrical model by experimental tests

Outdoor experimental tests can be useful for adjusting the parameters of the thermal-electrical model. The procedure to check the manufacturer power rating of commercial PV modules (obviously, they are without water cooling) requires to transfer the I–V curves measured at outdoor conditions of irradiance and cell temperature to STC. This correction is carried out thanks to equations provided by IEC Standard 60891 (2009). In the absence of water cooling, the cell temperature T_C reaches in outdoors values much higher than the STC temperature. In

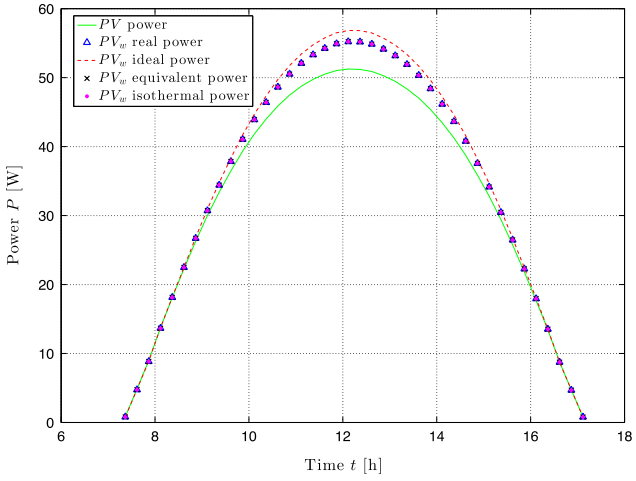

Fig. 13. Power profiles in January for Catania location with water flow rate $10\,\mathrm{l\,h^{-1}}$.

these tests (less than 1 s long), the temperature of the cells is uniform and a thermal equilibrium condition is recommended with constant irradiance, ambient temperature and wind speed for some minutes. The electrical characteristics can be obtained by the automatic data acquisition system described in Spertino et al. (2015). The typical uncertainties of measurement are around ±1%, ±0.1% and ±1% in terms of current, voltage and power, respectively. As an example of the procedure, the experimental results of a test on the PV module under study without cooling (i) and a test with water cooling (ii) are discussed below. In particular, before the measurements, an accurate cleaning of the PV module was performed to avoid the dirt of a big city (Torino, Italy) and dust typical of desert zone as in Rehman and El-Amin (2012).

(i) The steady-state ambient conditions (Spertino et al., 2015) were $G = 960 \pm 20$ W m^{-2}, $T_a = 286 \pm 0.2$ K, with negligible wind speed, and the cell temperature $T_C = 322 \pm 2$ K was derived by the thermal model. Figs. 10 and 12 show the I–V and P–V curves in the previous conditions (green color) and after correction to the STC (red color).

(ii) In the same Figs. 10 and 12 the I–V and P–V curves (blue color) at $G = 1000 \pm 20$ W m^{-2}, $T_a = 288 \pm 0.2$ K are reported. In this condition, the power improvement is evident and it is ≈18%. The behavior of the coolant is displayed in Fig. 11 (dashed curve in blue), where the measured water temperature is $T_{inw} = 294.4 \pm 0.2$ K, at the inlet, and the thermal profile was simulated by the thermal model with water volume flow-rate $\dot{v} = 50$ l/h. Here, the cell temperature gradient is within the 296.8–299.8 ± 2 K and the mean value is very close to STC condition. It is worth noting that this thermal gradient does not generate power losses (due to electrical mismatch) in the corresponding I–V and P–V curves with water cooling. This fact can be deduced by an almost perfect agreement between the I–V and P–V curves (Figs. 10 and 12) corrected to STC without cooling and the I–V and P–V curves (Figs. 10 and 12) with water cooling which reproduce in outdoor the STC. The existing electrical mismatch in the module cells does not cause power reduction, because the cells are connected in series and the mismatch occurs only in the cell voltages.

Furthermore, Fig. 12 shows the experimental P–V curve of the module without cooling corrected at STC (in red color, as in Fig. 10) and the experimental P–V curve of the module with water cooling (in blue color). Also in this case of power curves, the agreement is very satisfying. For this reason, it is possible to estimate all electrical parameters and compare them with the STC data declared by the manufacturer. The results are reported in Table 4,

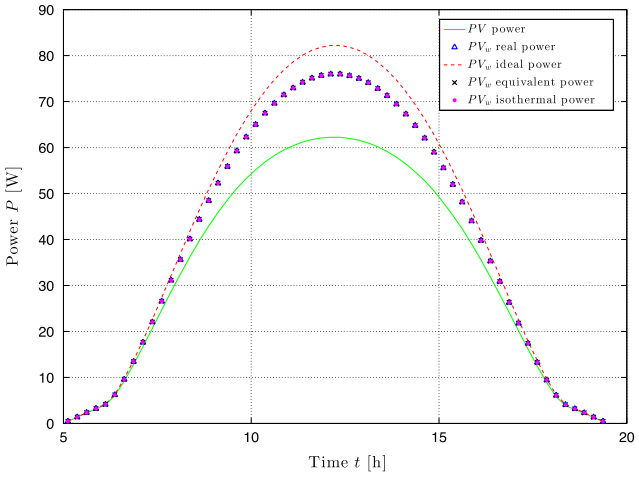

Fig. 14. Power profiles in July for Catania location with water flow rate 10 l h^{-1}.

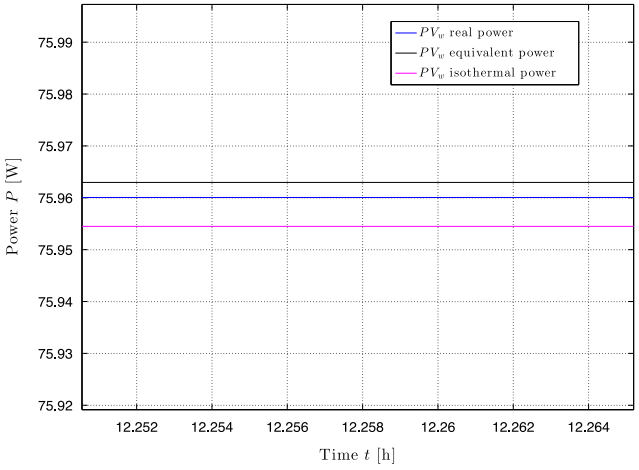

Fig. 15. Power profiles: larger view.

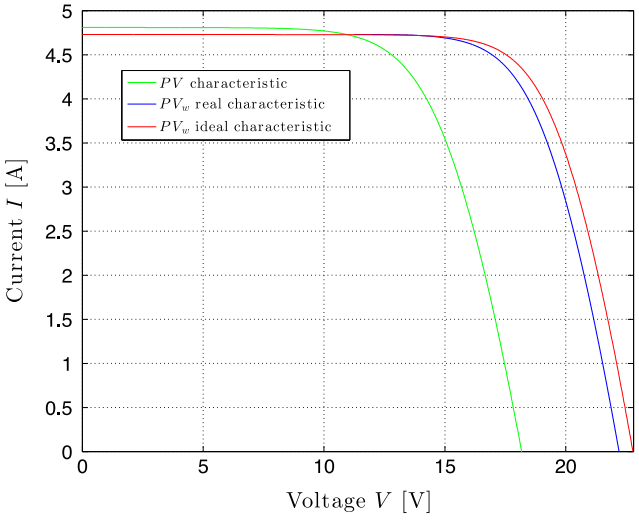

Fig. 16. Simulated I–V curves with water flow rate of 30 l h^{-1}.

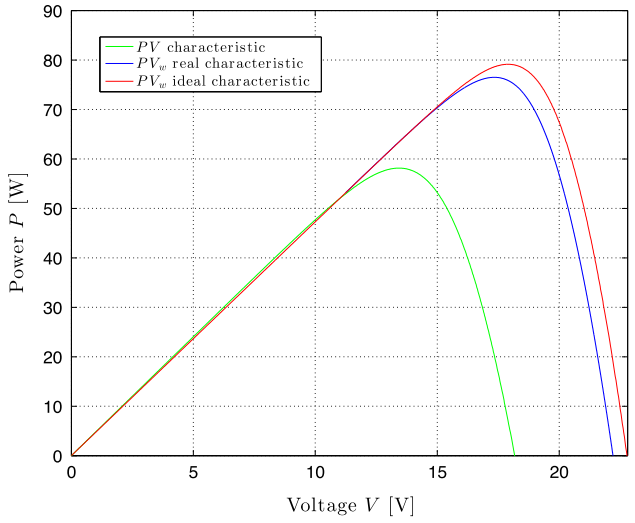

Fig. 17. Simulated P–V curves with water flow rate of $30\,\mathrm{l\,h^{-1}}$.

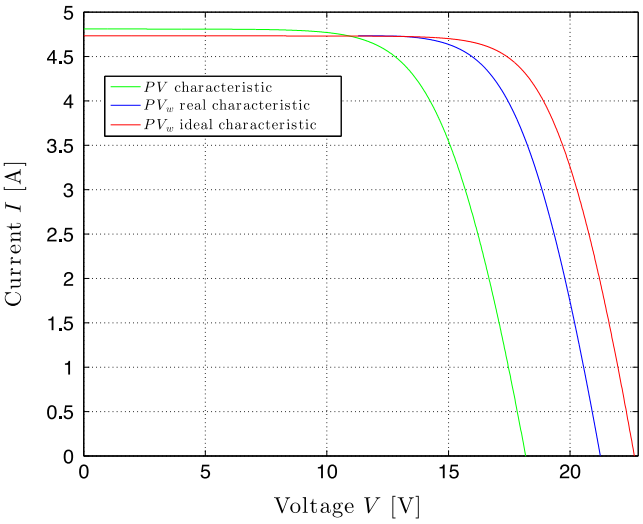

Fig. 18. Simulated I–V curves with $10\,\mathrm{l\,h^{-1}}$coolant flow rate.

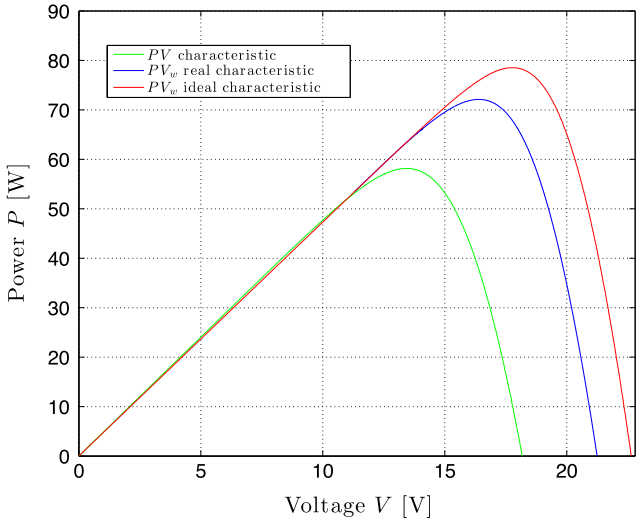

Fig. 19. Simulated P–V curves with $10\,\mathrm{l\,h^{-1}}$ coolant flow rate.

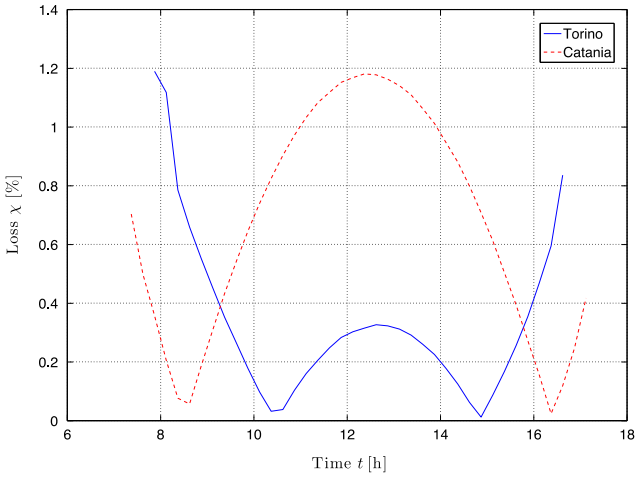

Fig. 20. Simulated power losses in January. Coolant flow rate $30\,\mathrm{l\,h^{-1}}$.

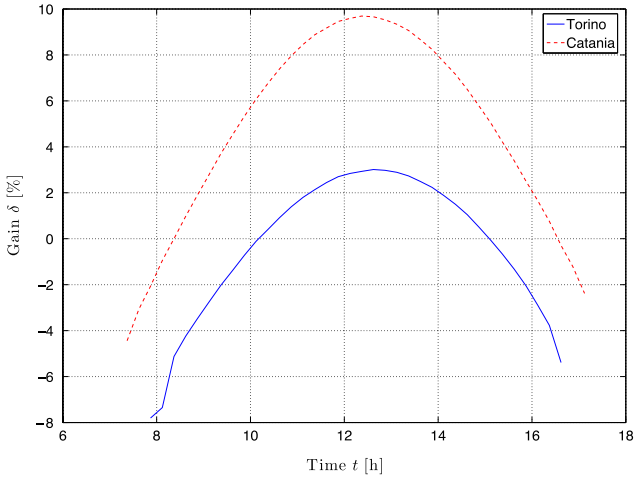

Fig. 21. Simulated power gain in January. Coolant flow rate $30\,\mathrm{l\,h^{-1}}$.

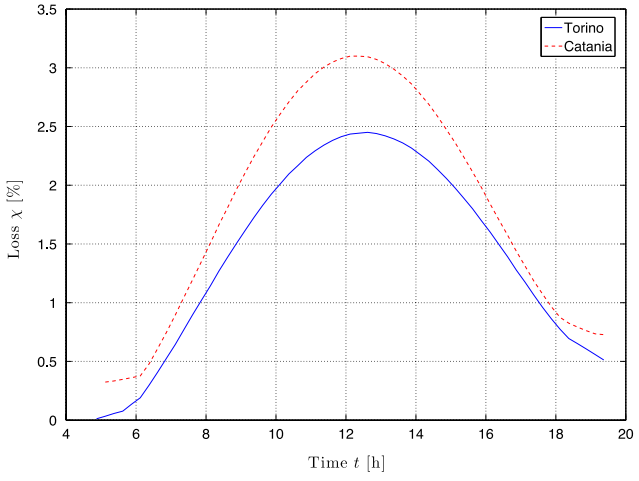

Fig. 22. Simulated power losses in July. Coolant flow rate $30\,\mathrm{l\,h^{-1}}$.

where a significant reduction of the estimated maximum power at STC (about -10%) is observed with respect to the manufacturer data.

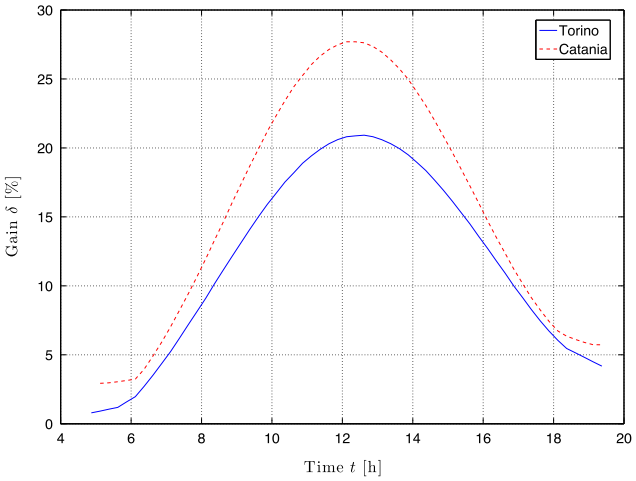

Fig. 23. Simulated power gain in July. Coolant flow rate 30 l h^{-1}.

7. Simulation results obtained with and without cooling on PV module

On the basis of the described experimental procedure, a simulation has been carried out with the parameters of cell equivalent circuit adjusted by the outdoor testing. Daily power profiles are simulated without coolant (PV power) and with coolant (PV$_w$ power) in four conditions, as follows.

(i) *power in ideal conditions (PV$_w$ ideal power)*, where the cell temperatures in all the rows are equal to the temperature of the first cell row (i.e., the minimum value).
(ii) *power without electrical mismatch (PV$_w$ equivalent power)*, where the MPP of each cell row is calculated separately, assuming that every row is working independently from the other rows, i.e., without electrical mismatch.
(iii) *power with electrical mismatch (PV$_w$ real power)*, where the cell rows of the PV module are simulated with their proper thermal and electrical parameters.
(iv) *power with mean temperature (PV$_w$ isothermal power)*, assuming that all PV cells operate with a constant temperature equal to the mean temperature previously calculated. In thermal phenomena one should use logarithmic mean temperature, but the cell-row temperatures and water temperatures exhibit almost linear profiles, as reported in Fig. 11, so the arithmetic mean temperature was used instead.

Conditions 2–4 are particularly important for the purposes of this paper. In presence of the coolant flow, there is a thermal gradient among the cell rows with different temperatures in operation. As a consequence, there are different voltages and currents at maximum power V_{mpp} and I_{mpp}, respectively. However, there is a negligible difference between the cases with and without electrical mismatch, and the equivalent case without thermal gradient at arithmetic mean temperature.

Numerical simulations are first reported in Figs. 13–15 for a location (Catania, in Sicily) in which the water cooling has a remarkable impact to enhance the PV efficiency and in turn the energy production. The PV module behavior is investigated in winter (January) and in summer (July). The I–V curves are calculated by the experimentally adjusted parameters without coolant and with coolant (flow rate of 10 l/h) in four cooling conditions. Thus, it is possible to evaluate the power difference between the two cases, where the thermal gradient occurs with and without electrical mismatch, and the isothermal case with arithmetic mean temperature. They differ by less than 10^{-2} W (0.013%) in peak condition, as shown in Fig. 15. The maximum power gain δ[%], due to the coolant effect, is:

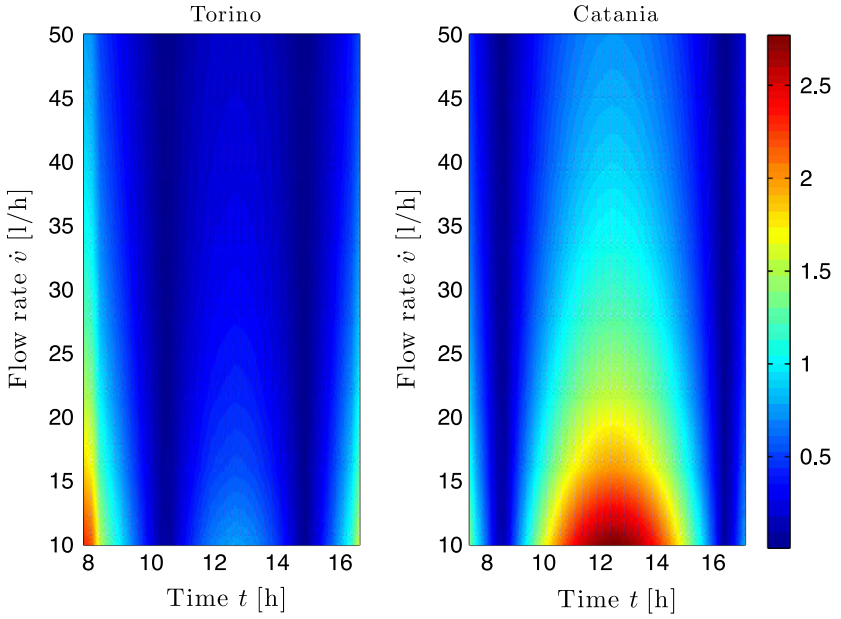

Fig. 24. Simulated power losses in January in percent.

$$\delta[\%] = \frac{P_{\mathrm{I}} - P_{\mathrm{NC}}}{P_{\mathrm{NC}}} 100 \tag{44}$$

where P_{I} is the ideal electric power with coolant and P_{NC} is the power without coolant. In the real condition a temperature gradient among the cell rows exists. The power loss $\chi[\%]$, as a consequence of this effect, can be calculated with respect to the ideal conditions:

$$\chi[\%] = \frac{P_{\mathrm{R}} - P_{\mathrm{I}}}{P_{\mathrm{I}}} 100 \tag{45}$$

where P_{R} is the power produced in real conditions. Taking into account all effects, the real power gain $\xi[\%]$ is:

$$\xi[\%] = \frac{P_{\mathrm{R}} - P_{\mathrm{NC}}}{P_{\mathrm{NC}}} 100 \tag{46}$$

The I–V and P–V curves in Figs. 16 and 17, respectively, are obtained with cooling, both in ideal and real conditions, and without coolant, at $G = 1000\ \mathrm{W/m^2}$, $T_{\mathrm{a}} = 305\ \mathrm{K}$. Noticeable differences between real and no coolant conditions confirm the advantage of this PV solution with respect to the usual solution, where only the natural air circulation leads to PV cooling. With $\dot{v} = 30\ \mathrm{l/h}$ the power loss is $\chi = -3\%$ with respect to the ideal case and the power gain is $\xi = 26.5\%$. If $\dot{v} = 10\ \mathrm{l/h}$ (Figs. 18 and 19), the power loss $\chi = -7\%$ and the power

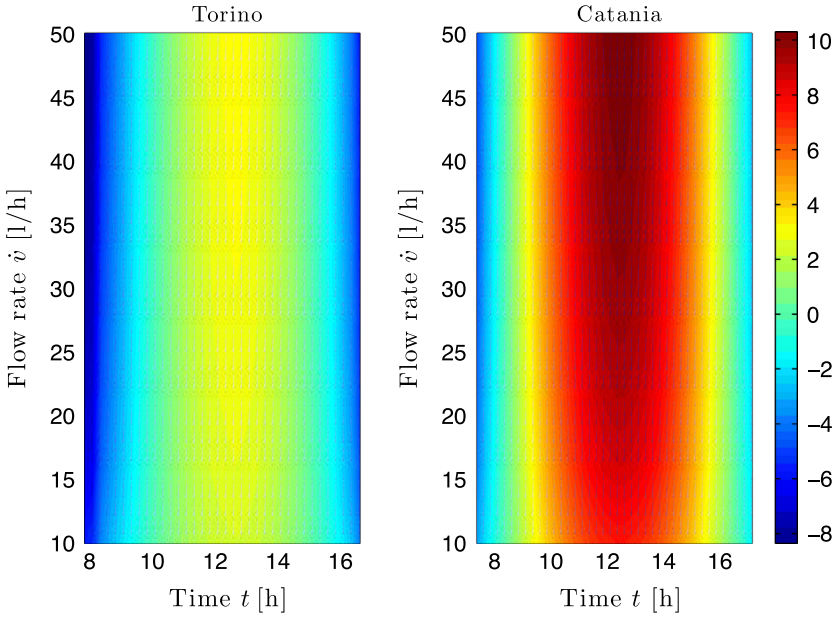

Fig. 25. Simulated power gain in January in percent.

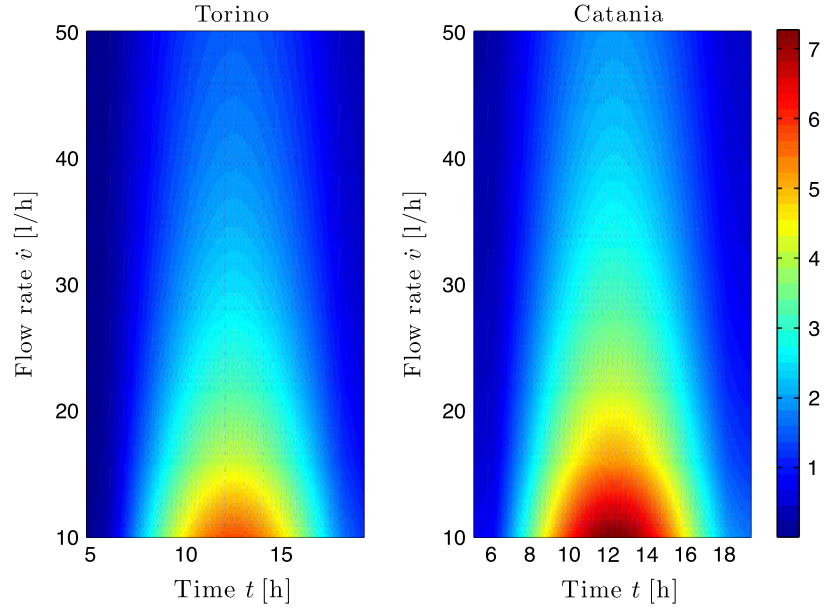

Fig. 26. Simulated power losses in July in percent.

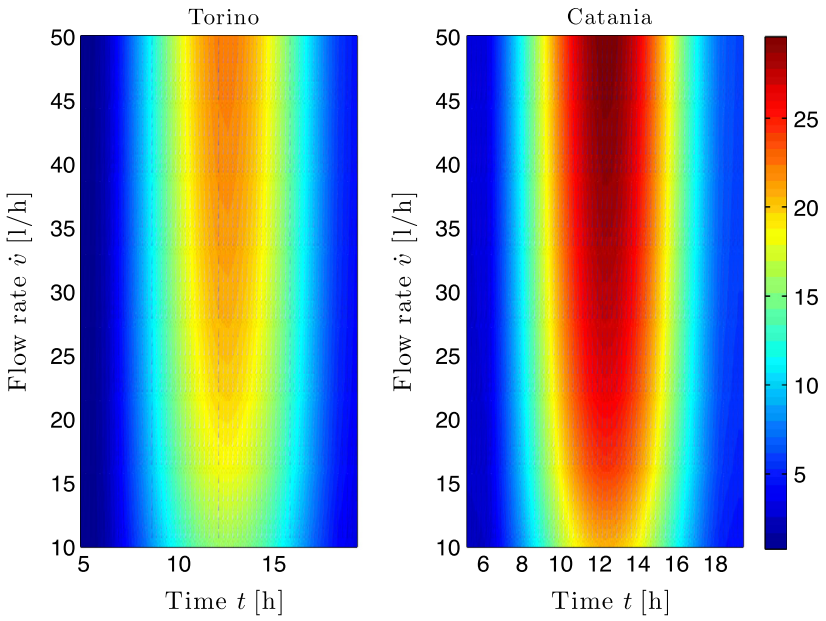

Fig. 27. Simulated power gain in July in percent.

gain is $\xi = 19.8\%$. In the two cases the ideal power gains δ are 30.4% and 28.9%, respectively. A lower coolant flow-rate means higher power losses as a consequence of thermal gradient and lower power gain for higher cell-row temperatures.

Changing the values of G, T_a and $\dot{v}$, a complete map of loss and gain factors has been obtained. Generally, G and T_a are correlated and depend on the geographical site. Loss and gain factors are calculated for the average day of each month, with different flow rates for Catania and Torino (a location Northwestern Italy with very different climatic conditions). In Figs. 20–23, where solid lines refer to Torino, and dashed lines to Catania, the simulations are reported with flow rate $\dot{v} = 30$ l/h for January and July. The defined power gain/loss parameters show a strong symmetry with respect to noon. The gain reaches its maximum value (28% in Catania and 21% in Torino) around noon. The minimum value (may be negative in winter), conversely, occurs close to the beginning and the end of the day. In winter the loss factor exhibits an initial decreasing trend, and after reaching a minimum increases again until noon. Indeed, the cell temperature is lower than the coolant inlet temperature and the system has a reversed behavior. The cell rows are warmed up, and the efficiency

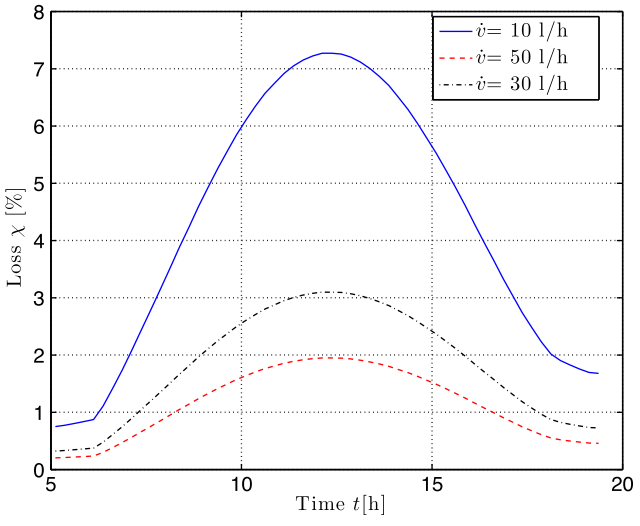

Fig. 28. Simulated percent losses in Catania, July for 10, 30 and 50 l h^{-1} coolant flow.

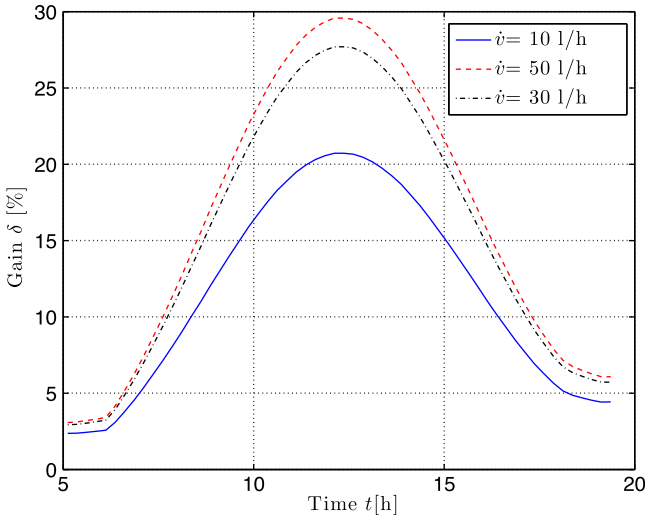

Fig. 29. Simulated percent gains in Catania, July for 10, 30 and 50 l h^{-1} coolant flow.

of the PV module decreases. In these cases the coolant system must be definitely switched off.

The significant increment of loss factor in Catania in summer means that the thermal gradient among the PV cell rows is higher. This finding suggests that, in this case, an increase of coolant flow rate may substantially improve the electrical performance.

In order to investigate the influence of the coolant flow rate on loss/gain factors, a complete set of simulations is carried out for both Catania and Torino, for flow rates within 10–50 l/h.

Results are reported in Figs. 24–27 for January and July. In these figures, the influence of the flow rate is clear. In a city with a warmer climate (Catania) the loss factor reaches values around 7% in July when the flow rate is low (10 l/h), and the gain factor reaches values near to 30% with 50 l/h flow rate. Furthermore, the performance rapidly improves when the flow rate rises from 10 l/h to 30 l/h. With a flow rate of 50 l/h, performance improvements are less evident. These findings are confirmed in Figs. 28 and 29, where the loss and gain factors are reported for three values of flow rate. A flow rate of 30 l/h seems to be a good compromise solution, because the performance is only slightly lower than in the 50 l/h case, while the electrical consumption of the circulation pump is about 4.6 times smaller.

8. Conclusions

In order to indirectly measure, as accurately as possible, the cell temperature, a PV module has been manufactured ad hoc with the option of water cooling. Thanks to the information about the geometrical dimensions and the physical characteristics of the materials in the PV module, a detailed thermal–electrical model has been built and adjusted by experimental tests. Particular attention has been devoted to the simulation of all the mechanisms of heat transfer.

With the water cooling option the improvement of PV module performance takes into account the thermal gradient consequent to the coolant flow. Experimental tests clarify that the thermal gradient produces a negligible electrical mismatch in a PV generator where the series connection is used. The simulations point out that the energy gain is remarkable in summer in locations with different climates and strongly depends on the flow rate. Numerical results show that the coolant must be activated according to the location and the season of the year, and in some cases its usage must be avoided. The topic of further investigations will be focused on a detailed analysis considering an entire PV system with circulation pump and water distribution system for an optimum technical–economical flow rate.

An important result, reached using a water cooled PV module, regards the ability to reproduce the STC conditions which are not feasible with the PV modules subject to natural air circulation. In this way, it is possible to verify the STC manufacturer data through simple outdoor tests. These results suggest developing a new procedure for the assessment of the PV-module nominal performance.

Acknowledgments

The authors gratefully acknowledge B.Sc. Lorenzo Ghiringhello who has built and tested the PV module under study in this paper.

Appendix A

A.1. Matrix **A** *and vector* ***b*** *used in the solution of the linear system of equations in Section 4.1.1*

$$\mathbf{A}=\begin{bmatrix} h_r+h_{conv}+\frac{k_{PC}}{s_1} & -\frac{k_{PC}}{s_1} & 0 & 0 & 0 & 0 & 0 \\ -\frac{k_{PC}}{s_1} & \frac{k_{PC}}{s_1}+\frac{k_{TPU}}{s_2} & -\frac{k_{TPU}}{s_2} & 0 & 0 & 0 & 0 \\ 0 & -\frac{k_{TPU}}{s_2} & \frac{k_{TPU}}{s_2}+\frac{k_{TPU}}{s_4} & -\frac{k_{TPU}}{s_4} & 0 & 0 & 0 \\ 0 & 0 & -\frac{k_{TPU}}{s_4} & U_{alv}+\frac{k_{TPU}}{s_4} & -U_{alv} & 0 & 0 \\ 0 & 0 & 0 & -U_{alv} & U_{ag}+U_{alv} & -U_{ag} & 0 \\ 0 & 0 & 0 & 0 & -U_{ag} & U_{ag}+\frac{k_{PC}}{s_7} & -\frac{k_{PC}}{s_7} \\ 0 & 0 & 0 & 0 & 0 & -\frac{k_{PC}}{s_7} & h_{r1}+h_{conv}+\frac{k_{PC}}{s_7} \end{bmatrix} \tag{A1}$$

$$\mathbf{b}=\begin{bmatrix} h_r T_{sky}+h_{conv}T_a \\ [(2-\eta_{el})\tau_{ARC}-1]\tau_{PC}\tau_{TPU1}G \\ 0 \\ 0 \\ 0 \\ h_{r1}T_{sky}+h_{conv}T_a \end{bmatrix} \tag{A2}$$

A.2. Matrix $\mathbf{A}_Z$ and vector $\mathbf{b}_Z$ used in the solution of the linear system of equations in Section 4.1.2

$$\mathbf{A}_Z = \begin{bmatrix}
h_r + h_{conv} + \frac{k_{PC}}{s_1} & -\frac{k_{PC}}{s_1} & 0 & 0 & 0 & 0 & 0 & 0 & 0 & 0 \\
-\frac{k_{PC}}{s_1} & \frac{k_{PC}}{s_1} + \frac{k_{TPU}}{s_2} & -\frac{k_{TPU}}{s_2} & 0 & 0 & 0 & 0 & 0 & 0 & 0 \\
0 & -\frac{k_{TPU}}{s_2} & \frac{k_{TPU}}{s_2} + \frac{k_{TPU}}{s_4} & -\frac{k_{TPU}}{s_4} & 0 & 0 & 0 & 0 & 0 & 0 \\
0 & 0 & -\frac{k_{TPU}}{s_4} & \frac{k_{PC}}{s_{PC}} + \frac{k_{TPU}}{S_4} & -\frac{k_{PC}}{S_{PC}} & 0 & 0 & 0 & 0 & 0 \\
0 & 0 & 0 & -\frac{k_{PC}}{S_{PC}} & \frac{k_{PC}}{S_{PC}} + h_w & 0 & 0 & 0 & 0 & 0 \\
0 & 0 & 0 & 0 & h_w & -\frac{\dot{v}\cdot c}{Y} & h_w & 0 & 0 & 0 \\
0 & 0 & 0 & 0 & 0 & h_w & \frac{k_{PC}}{S_{PC}} + h_w & -\frac{k_{PC}}{S_{PC}} & 0 & 0 \\
0 & 0 & 0 & 0 & 0 & 0 & -\frac{k_{PC}}{S_{PC}} & \frac{k_{PC}}{S_{PC}} + U_{ag} & -U_{ag} & 0 \\
0 & 0 & 0 & 0 & 0 & 0 & 0 & -U_{ag} & U_{ag} + \frac{k_{PC}}{s_7} & -\frac{k_{PC}}{S_7} \\
0 & 0 & 0 & 0 & 0 & 0 & 0 & 0 & -\frac{K_{PC}}{S_7} & h_r + h_{conv} + \frac{k_{PC}}{s_1}
\end{bmatrix} \tag{A3}$$

$$\mathbf{b}_Z = \begin{bmatrix}
h_r T_{sky} + h_{conv} T_a \\
0 \\
[(2-\eta_{el})\tau_{ARC} - 1]\tau_{PC}\tau_{TPU1} G \\
0 \\
h_w T_w \\
-2h_w T_w \\
h_w T_w \\
0 \\
0 \\
h_{r1} T_{sky} + h_{conv} T_a
\end{bmatrix} \tag{A4}$$

References

Abdolzadeh, M., Ameri, M., 2009. Improving the effectiveness of a photovoltaic water pumping system by spraying water over the front of photovoltaic cells. Renew. Energy 34, 91–96.

ASHRAE (American Society of Heating, Refrigeration, Air Conditioning Engineers) handbook: HVAC applications, 1999. Atlanta (GA).

Andrei, H., Nicolaescu, G., Radulescu, S., Andrei, P.C., 2013. New approach of PV cell efficiency. Proceedings of 12th International Conference on Environment and Electrical Engineering (EEEIC 2013), Wroclaw, Poland, May 5–8, pp. 106–111.

ASTM, 1998. Standard E1036. Standard Test Methods for Electrical Performance of Non-Concentrator Terrestrial Photovoltaic Modules ad Arrays Using Reference Cells. The American Society for Testing and Materials, West Conshohocken, PA, USA.

Attivissimo, F., Adamo, F., Carullo, A., Lanzolla, A.M.L., Spertino, F., Vallan, A., 2013. On the performance of the double-diode model in estimating the maximum power point for different photovoltaic technologies. Measurement 46, 3549–3559.

Ayedh, H., Qahtani, A.L., Abuhamdeh, M.S., Alsmadi, Y.M., 2012. A simplified and comprehensive approach to characterize photovoltaic system performance. IEEE Energytech, 1–6.

Bahaidarah, H., Subhan, A., Gandhidasan, P., Rehman, S., 2013. Performance evaluation of a PV (photovoltaic) module by back surface water cooling for hot climatic conditions. Energy 59, 445–453.

Bellia, H., Youcef, R., Fatima, M., 2014. A detailed modeling of photovoltaic module using MATLAB. NRIAG J. Astron. Geophys. 3, 53–61.

Ben Cheikh el Hocine, H., Touafek, K., Kerrour, F., Haloui, H., Khelifa, A., 2015. Model validation of an empirical photovoltaic thermal (PV/T) collector. International Conference on Technologies and Materials for Renewable Energy, Environment and Sustainability, TMREES15, Energy Procedia 74, 1090–1099.

Bernards, J., 2004. Èngie solaire Calculs et optimisation. Ellipses Pub. House, France.

Brinkworth, B., Sandberg, M., 2006. Design procedure for cooling ducts to minimize efficiency loss due to temperature rise in PV arrays. Sol. Energy 80, 89–103.

bSolar GmbH, Link to a Manufacturer of Solar Cells. Web site: <http://www.b-solar.com/Pictures/Monofacial%20TG18.5BR_D200.pdf> (accessed 6.01.15).

Çengel, Y.A., Turner, R.H., 2001. Thermal-Fluid Sciences. McGraw-Hill, New York.

Chatterjee, A., Keyhani, A., 2011. Thevenin's equivalent of photovoltaic source models for MPPT and power grid studies. Proceedings of the IEEE Power and Energy Society General Meeting, Detroit, MI, USA, July 24–29, pp. 1–7.

Chen, H., Chen, X., Li, S., Ding, H., 2014. Comparative study on the performance improvement of photovoltaic panel with passive cooling under natural ventilation. Int. J. Smart Grid Clean Energy 3, 374–379.

Chow, T.T., 2010. A review on photovoltaic/thermal hybrid solar technology. Appl. Energy 87, 365–379.

Coleman, T.F., Li, Y., 1996. An interior, trust region approach for nonlinear minimization subject to bounds. SIAM J. Optim. 6, 418–445.

De Soto, W., Klein, S.A., Beckman, W.A., 2006. Improvement and validation of a model for photovoltaic array performance. Sol. Energy 80, 78–88.

Du, D., Darkwa, J., Kokogiannakis, G., 2013. Thermal management systems for photovoltaics (PV) installations: a critical review. Sol. Energy 97, 238–254.
Duffie, J.A., Beckman, W.A., 1974. Solar Energy Thermal Processes. Wiley-Interscience, New York, London.
Elnozahya, A., Rahmana, A.K.A., Alib, A.H.H., Abdel-Salamc, M., Ookawara, S., 2015. Performance of a PV module integrated with standalone building in hot arid areas as enhanced by surface cooling and cleaning. Energy Build. 88, 100–109.
Evans, D.L., 1981. Simplified method for predicting photovoltaic array output. Sol. Energy 27, 555–560.
Farivar, G., Asaei, B., 2010. Photovoltaic module single diode model parameters extraction based on manufacturer datasheet parameters. Proceedings of the IEEE International Conference on Power and Energy, Kuala Lumpur, Malaysia, November 29–December 1, pp. 929–934.
Florschuetz, L.W., 1975. On heat rejection from terrestrial solar cell arrays with sunlight concentration. Proceedings of the 11th Photovoltaic Specialists Conference Record Mater, Scottsdale, Arizona, May, pp. 318–326.
Gang, P., Jie, J., Wei B, H., Keliang, L., Hanfeng, H., 2007. Performance of photovoltaic solar assisted heat pump system in typical climate zone. J. Energy Environ. 6, 1–9.
Holman, J.P., 2010. Heat Transfer. tenth ed. McGraw-Hill Book Company.
IEC Standard 60891, 2009. Procedures for temperature and irradiance corrections to measured *I–V* characteristics of crystalline silicon PV devices.
IEC 61215, 2005. Crystalline silicon terrestrial photovoltaic (PV) modules – design qualification and type approval. In: 2nd Edition of International Electrotechnical Commission, Italy, pp. 1–16.
Kalogirou, S.A., Tripanagnostopoulos, Y., 2006. Hybrid PV/T solar systems for domestic hot water and electricity production. Energy Convers. Manage. 47, 3368–3382.
Karatepe, E., Boztepe, M., Çolak, M., 2007. Development of a suitable model for characterizing photovoltaic arrays with shaded solar cells. Sol. Energy 81, 977–992.
Kawamura, T., Harada, K., Ishihara, Y., Todaka, T., Oshiro, T., Nakamura, H., Imataki, M., 1997. Analysis of MPPT characteristics in photovoltaic power system. Sol. Energy Mater. Sol. Cells 47, 155–165.
Krauter, S.C.W., 2004. Development of an integrated solar home system. Sol. Energy Mater. Sol. Cells 82, 119–130.
Lasich, J.B., 2002. Cooling Circuit for Receiver of Solar Radiation. Australia Patent, WO02080286. Web site: <http://www.google.com/-patents/US7076965>
Lasnier, F., Ang, G., 1990. Photovoltaic Engineering Handbook. Adam Hilger, Bristol.
Leow, W.Z., Irwan, Y.M., Irwanto, M., Gomesh, N., Safwati, I., 2014. PIC 18F4550 controlled solar panel cooling system using DC hybrid. J. Sci. Res. Rep. 3, 2801–2816.
Lienhard, J.M., Lienhard, J.M., 2015. A Heat transfer textbook. fourth ed. Phlogiston Press.
Liu, S., Dougal, R.A., 2002. Dynamic multiphysics model for solar array. IEEE Trans. Energy Convers. 17, 285–294.
Makki, A., Omer, S., Sabir, H., 2015. Advancements in hybrid photovoltaic systems for enhanced solar cells performance. Renew. Sustain. Energy Rev. 41, 658–684.
Martín, N., Ruiz, J.M., 1999. A new method for the spectral characterization of PV module. Prog. Photovolt: Res. Appl. 7 (4), 299–310.
Messenger, R.A., Ventre, J., 2004. Photovoltaic Systems Engineering. second ed. CRC Press.
Millman, J., Grabel, A., 1987. Microelectronics. second ed. McGraw-Hill International Editions.
Moballegh, S., Jiang, J., 2011. Partial shading modeling of photovoltaic system with experimental validations. Power and Energy Society General Meeting, San Diego, CA, July 24–29, pp. 1–9.
Moharram, K.A., Abd-Elhady, M.S., Kandil, H.A., El-Sherif, H., 2013. Enhancing the performance of photovoltaic panels by water cooling. Ain Shams Eng. J. 4, 869–877.
Myers, D.R., Emery, K., Gueymard, C., 2002. Revising and validating spectral irradiance reference standards for photovoltaic performance. Proceedings of the ASES/ASME Solar Conference, June, Reno, Nevada, June 15–20, pp. 1–10.
Nayak, B.K., Mohapatra, A., Mohanty, K.B., 2013. Parameters estimation of photovoltaic module using nonlinear least square algorithm: a comparative study. Annual IEEE India Conference (INDICON), Mumbai, India, December 13–15, pp. 1–6.
Nolay, P., 1987. Développement d'une méthode générale d'analyse des systèmes photovoltaïques. Doctoral dissertation.
Notton, G., Cristofari, C., Mattei, M., Poggi, P., 2005. Modelling of a double-glass photovoltaic module using finite differences. Appl. Therm. Eng. 25, 2854–2877.
Omubo-Pepple, V.B., Israel-Cookey, C., Alaminokuma, G.I., 2009. Effects of temperature, solar flux and relative humidity on the efficient conversion of solar energy to electricity. Eur. J. Sci. Res. 35, 173–180.
Park, M., Yu, I.K., 2004. A novel real-time simulation technique of photovoltaic generation systems using RTDS. IEEE Trans. Energy Convers. 19, 164–169.
Patel, M.R., 1999. Wind and Solar Power Systems. CRC Press, New York.
Picault, D., Raison, B., Bacha, S., de la Casa, J., Aguilera, J., 2010. Forecasting photovoltaic array power production subject to mismatch losses. Sol. Energy 84, 1301–1309.
Pierro, M., Bucci, F., Cornaro, C., 2015. Full characterization of photovoltaic modules in real operating conditions: theoretical model, measurement method and results. Prog. Photovolt: Res. Appl. 23, 443–461.
Platz, R., Fischer, D., Zufferey, M.A., Selvan, J.A.A., Haller, A., Shah, A., 1997. Hybrid collectors using thin-film technology. Proceeding of the Photovoltaic Specialists Conference, Conference Record of the Twenty-Sixth IEEE, Anaheim, California, September 29–October 3, pp. 1293–1296.
Rauschenbach, H.S., 1980. Solar Cell Array Design Handbook: The Principles and Technology of Photovoltaic Energy Conversion. Springer.
Rehman, S., El-Amin, I., 2012. Performance evaluation of an off-grid photovoltaic system in Saudi Arabia. Energy 46, 451–458.
Rossi, C., Tagliafico, L.A., Scarpa, F., Bianco, V., 2013. Experimental and numerical results from hybrid retrofitted photovoltaic panels. Energy Convers. Manage. 76, 634–644.
Royne, A., Dey, C.J., Mills, D.R., 2005. Cooling of photovoltaic cells under concentrated illumination: a critical review. Sol. Energy Mater. Sol. Cells 86, 451–483.
Salih, S.M., Abd, O.I., Abid, K.W., 2015. Performance enhancement of PV array based on water spraying technique. Int. J. Sustain. Green Energy 4, 8–13.
SEI, 2004. Photovoltaics Design & Installation Manual. New Society Publishers.
Siddique, H.A.B., Xu, P., De Doncker, R.W., 2013. Parameter extraction algorithm for one-diode model of PV panels based on datasheet values. Proceeding of 4th International Conference on Clean Electrical Power: Renewable Energy Resources Impact, ICCEP, Alghero, Italy, June 11–13, pp. 7–13.
Skoplaki, E., Palyvos, J.A., 2009. On the temperature dependence of photovoltaic module electrical performance: a review of efficiency/power correlations. Sol. Energy 83, 614–624.
Shongwe, S., 2015. Comparative analysis of different single-diode PV modeling methods. IEEE J. Photovoltaics 5, 938–946.
Spertino, F., D'Angola, A., Fracastoro, G., Enescu, D., Zaffina, R., 2014. A new photovoltaic–thermal hybrid module: thermal electric model and experimental tests. University Power Engineering Conference (UPEC). Cluj-Napoca, Romania, September 2–5, pp. 1–6.

Spertino, F., Ahmad, J., Ciocia, A., Di Leo, P., Murtaza, A.F., Chiaberge, M., 2015. Capacitor charging method for *I–V* curve tracer and MPPT in photovoltaic systems. Sol. Energy 119, 461–473.

Suresh, V., Naviynkumar, S., Kirubakaran, V., 2013. Improved power output of PV system by low cost evaporative cooling technology. International Conference on Green Computing, Communication and Conservation of Energy (ICGCE), Chennai, India, December 12–14, pp. 640–643.

Teo, H.G., Lee, P.S., Hawlader, M.N.A., 2012. An active cooling system for photovoltaic modules. Appl. Energy 90, 309–315.

Tiwari, G.N., Dubey, S., 2010. Fundamentals of Photovoltaic Modules and their Applications. Royal Society of Chemistry (RSC), Cambridge.

Ueda, Y., Sakurai, T., Tatebe, S., Itoh, A., Kurokawa, K., 2008. Performance analysis of PV systems on the water. EU PVSEC Conference, Valencia, Spain, September 1–5, pp. 2670–2673.

Valeh-e-Sheyda, P., Rahimi, M., Karimi, E., Asadi, M., 2013. Application of two-phase flow for cooling of hybrid microchannel PV cells: a comparative study. Energy Convers. Manage. 69, 122–130.

Villalva, M.G., Gazoli, J.R., Filho, E.R., 2009. Comprehensive approach to modeling and simulation of photovoltaic arrays. IEEE Trans. Power Electr. 24, 1198–1208.

Walker, G., 2001. Evaluating MPPT converter topologies using a Matlab PV model. J. Electr. Electr. Eng., 1–6

Xiao, W., Dunford, W.G., Capel, A., 2004. A novel modeling method for photovoltaic cells. In: Proceeding of 35th Annual IEEE Power Electronics Specialists Conference (PESC), Aachen, Germany, June 20–25, vol. 3, pp. 1950–1956.

Xu, G.Y., Deng, S.M., Zhang, X.S., 2009. Simulation of a photovoltaic/thermal heat pump system having a modified collector/evaporator. Sol. Energy 83, 1967–1976.

Ye, Z., Nobre, A., Reindl, T., Luther, J., Reise, C., 2013. On PV module temperatures in tropical regions. Sol. Energy 88, 80–87.

Zhao, X., Zhang, X., Riffat, S.B., Su, Y., 2011. Theoretical study of the performance of a novel PV/e roof module for heat pump operation. Energy Convers. Manage. 52, 603–614.

Zondag, H.A., 2008. Flat-plate PV–thermal collectors and systems: a review. Renew. Sustain. Energy Rev. 12, 891–959.

Zondag, H.A., de Vries, D.W., van Helden, W.G.J., van Zolingen, R.J.C., van Steenhoven, A.A., 2003. The yield of different combined PV–thermal collector designs. Sol. Energy 74, 253–269.